J Neurophysiol 116: 995–1011, 2016.
First published July 8, 2016; doi:10.1152/jn.01121.2015.

Two classes of excitatory synaptic responses in rat thalamic reticular neurons

Charlotte Deleuze and John R. Huguenard
Department of Neurology and Neurological Sciences, Stanford University School of Medicine, Stanford, California

Submitted 27 December 2015; accepted in final form 8 June 2016

Deleuze C, Huguenard JR. Two classes of excitatory synaptic responses in rat thalamic reticular neurons. *J Neurophysiol* 116: 995–1011, 2016. First published June 8, 2016; doi:10.1152/jn.01121.2015.—The thalamic reticular nucleus (nRt), composed of GABAergic cells providing inhibition of relay neurons in the dorsal thalamus, receives excitation from the neocortex and thalamus. The two excitatory pathways promoting feedback or feedforward inhibition of thalamocortical neurons contribute to sensory processing and rhythm generation. While synaptic inhibition within the nRt has been carefully characterized, little is known regarding the biophysics of synaptic excitation. To characterize the functional properties of thalamocortical and corticothalamic connections to the nRt, we recorded minimal electrically evoked excitatory postsynaptic currents from nRt cells in vitro. A hierarchical clustering algorithm distinguished two types of events. Type 1 events had larger amplitudes and faster kinetics, largely mediated by α-amino-3-hydroxy-5-methyl-4-isoxazolepropionic acid (AMPA) receptors, whereas type 2 responses had more prominent *N*-methyl-D-aspartate (NMDA) receptor contribution. Type 1 responses showed subnormal axonal propagation and paired pulse depression, consistent with thalamocortical inputs. Furthermore, responses kinetically similar to type 1 events were evoked by glutamate-mediated activation of thalamic neurons. Type 2 responses, in contrast, likely arise from corticothalamic inputs, with larger NMDA conductance and weak Mg^{2+}-dependent block, suggesting that NMDA receptors are critical for the cortical excitation of reticular neurons. The long-lasting action of NMDA receptors would promote reticular cell burst firing and produce powerful inhibitory output to relay neurons proposed to be important in triggering epilepsy. This work provides the first complete voltage-clamp analysis of the kinetics and voltage dependence of AMPA and NMDA responses of thalamocortical and corticothalamic synapses in the nRt and will be critical in optimizing biologically realistic neural network models of thalamocortical circuits relevant to sensory processing and thalamocortical oscillations.

thalamocortical; corticothalamic; thalamic reticular nucleus; α-amino-3-hydroxy-5-methyl-4-isoxazolepropionic acid receptor; *N*-methyl-D-aspartate receptor

NEW & NOTEWORTHY

The thalamic reticular nucleus provides feedforward and feedback inhibition to thalamocortical relay neurons. A minimal stimulation approach was used to isolate and characterize the two main excitatory inputs from the cortex and thalamus to this nucleus. Thalamic inputs were larger and had faster α-amino-3-hydroxy-5-methyl-4-isoxazolepropionic acid receptor kinetics, promoting rapid feedback inhibition, whereas cortical inputs were kinetically slower and recruited a greater contribution from N-methyl-D-aspartate receptors, leading to more integrative feedback.

Address for reprint requests and other correspondence: J. R. Huguenard, Dept. of Neurology and Neurological Sciences, Stanford Univ. School of Medicine, Stanford, CA 94305 (e-mail: John.Huguenard@stanford.edu).

IN THE THALAMOCORTICAL (TC) circuit, the thalamic reticular nucleus (nRt) is positioned in a central location to monitor cortical sensory processing and shape the excitability of thalamic cells [i.e their ability to transmit sensory information to the cortex (Pinault 2004)]. Corticothalamic (CT) and TC fibers carry excitatory inputs arising from layer 6 of the neocortex and thalamic relay nucleus, respectively, and both extend axon collaterals in the nRt and make synaptic contacts onto reticular inhibitory neurons (Bourassa et al. 1995; Harris 1987; Scheibel and Scheibel 1966). Reticular neurons inhibit TC cells and also inhibit and connect electrically to neighboring nRt cells (Cox et al. 1997; Crabtree 1996; Deleuze and Huguenard 2006; Landisman et al. 2002; Ohara and Lieberman 1985; Shu and McCormick 2002).

The reciprocal nRt-TC connectivity forms the basis of the rhythmically active intrathalamic circuit that is thought to be critical in the generation of sleep oscillatory activities such as spindles (Jacobsen et al. 2001; von Krosigk et al. 1993). During pathological conditions, portions of this circuit become hypersynchronous and contribute to the generation of generalized absence seizures (Avanzini et al. 1993; Huguenard and McCormick 2007; Meeren et al. 2009; Steriade et al. 1993), although the degree of hypersynchrony is controversial (Lerescheet al. 2012). The switch between normal and epileptic activity is dependent in part on the balance between excitatory and inhibitory neurotransmitter actions within the circuit (e.g., Paz et al. 2011). In addition, excitation of the nRt drives the modulation and integration of sensory processing (Crabtree et al. 1998; Hartings et al. 2000; Hartings et al. 2003), excitotoxicity (Friedberg and Ross 1993; Ross et al. 1995), and possibly pain (Kolhekar et al. 1997). Therefore, a more detailed knowledge of the nature and features of excitatory inputs to the nRt is critical for our understanding of how the thalamic circuit functions under physiological and pathological conditions and for developing realistic neural network models of TC activity.

Some properties of these two major CT and TC excitatory synaptic connections onto the nRt have been established, especially as far as their manifestations in voltage recordings. For example, paired recordings between TC and nRt cells have revealed a powerful thalamoreticular synaptic drive, with large unitary excitatory postsynaptic potentials (EPSPs) that have a significant *N*-methyl-D-aspartate receptor (NMDA) receptor (NMDAR) component, small voltage dependence, and no significant Mg^{2+} block at rest and could trigger spikes (Gentet and Ulrich 2003), whereas presumed CT to nRt connections are characterized by weaker, subthreshold EPSPs (Gentet and Ulrich 2004). A comparative study found that CT inputs evoked responses with a larger amplitude and greater quantal conductance in the nRt than in the dorsal thalamus, suggesting a strong synaptic drive (Golshani et al. 2001) that would recruit nRt-mediated feedforward inhibition of dorsal thalamic neu-

rons. These findings have been supported by recent results with optogenetic stimulation of cortical and/or thalamic fibers (Cruikshank et al. 2010; Olsen et al. 2012). Both TC and CT responses in the nRt have NMDA and non-NMDA components (Gentet and Ulrich 2003; Gentet and Ulrich 2004; Warren and Jones 1997). Synchronous optogenetic activation of presumed single TC and CT pathways leads to enhanced firing of nRt cells (Yizhar et al. 2011). In addition, TC responses tend to have faster axonal propagation (Liu et al. 2001; Swadlow 1990) and response kinetics (Liu et al. 2001). Short-term plasticity also differs between the two pathways. Indeed, repetitive stimulation promotes facilitation of CT responses (Beierlein and Connors 2002; Golshani et al. 2001) but depression of TC inputs onto cortical neurons (Beierlein and Connors 2002) and those carried by TC axon collaterals onto the nRt (Gentet and Ulrich 2003). CT terminals predominate on nRt cells (Liu and Jones 1999) but tend to be small and simple with only few release site (Golshani et al. 2001) that yield small, slowly decaying EPSCs (Paz et al. 2011), whereas TC terminals are larger and can be perforated (Jones 2002) with multiple release sites (Liu et al. 2001) and larger, more rapidly decaying EPSCs (Paz et al. 2011). Expression of the α-amino-3-hydroxy-5-methyl-4-isoxazolepropionic acid (AMPA) receptor (AMPAR) subunit GluA4 [previously referred to as GluR4 or GluR-D (Traynelis et al. 2010)] is particularly high at CT synapses (Golshani et al. 2001; Liu et al. 2001; Mineff and Weinberg 2000).

However, the precise properties of thalamoreticular and corticoreticular synaptic connections remain unknown, especially with regard to the voltage dependence and relative contributions of NMDARs and AMPARs to each type of response. Indeed, to date, the most detailed functional characterization has used mainly voltage recordings to characterize EPSP integration in nRt cells (Gentet and Ulrich 2003; Gentet and Ulrich 2004; Warren and Jones 1997) or optogenetic stimuli that generally provide synchronous activation of multiple inputs. In the present study, we used a minimal stimulation paradigm to activate putative single fiber CT and TC inputs onto nRt cells recorded in voltage clamp to determine the kinetics of activation and inactivation of synaptic ionotropic glutamate receptors. Using a clustering algorithm, we could define two populations of response, each with distinct properties, and a useful mathematical discriminant function that readily divides responses into one of two classes based simply on the kinetics of the voltage-clamp synaptic response recorded at −70 mV. Voltage-clamp analysis was used to characterize the voltage dependence, contribution of AMPARs and NMDARs, kinetics, and short-term plasticity of the two types of responses. Based on these properties and their correspondence with those of excitatory postsynaptic currents (EPSCs) induced by local glutamate applied to the cortex or thalamus in TC or thalamic slices, we propose that type 1 responses originate from the specific activation of thalamoreticular axons, whereas type 2 responses originate from corticoreticular inputs. The latter have a much more prominent NMDAR contribution that would promote a powerful cortical recruitment of nRt cells during concerted cortical activity, as is proposed to occur at the onset of TC seizures (Meeren et al. 2002).

METHODS

In vitro slice preparation. All experiments were carried out according to protocols approved by the Stanford Institutional Animal Care and Use Committee. Sprague-Dawley rats [postnatal day (P)12–P15] were used. Although thalamic axonal myelination is not complete in the rat until P44 (JACOBSON 1963), the intrinsic excitability and synaptic properties of rodent nRt cells are largely mature at this age; in mice, synaptic stimulation of the internal capsule produces an action potential and burst firing in nRt cells, and these responses mature and stabilize around P14, in terms of both latency to firing and the maximal response (Warren and Jones 1997). Animals were anesthetized with pentobarbital (50 mg/kg) and decapitated, and the brains were rapidly removed and immersed in an ice-cold (4°C) slicing solution containing (in mM) 234 sucrose, 2.5 KCl, 1.25 NaH_2PO_4, 10 $MgSO_4$, 0.5 $CaCl_2$, 26 $NaHCO_3$, and 11 glucose (equilibrated with 95% O_2 and 5% CO_2, pH 7.4). Horizontal thalamic slices (300 μm) containing the thalamic ventrobasal complex (VB) and reticular nucleus were cut with a Lancer Series 1000 vibratome (Vibratome, St. Louis, MO). In some cases, we cut TC slices (400 μm) as previously described (Agmon and Connors 1991; Agmon and Connors 1992). Slices were incubated, initially at 32°C for 1 h and then at room temperature, in artificial cerebrospinal fluid (ACSF) containing (in mM) 126 NaCl, 2.5 KCl, 1.25 NaH_2PO_4, 1 $MgCl_2$, 2 $CaCl_2$, 26 $NaHCO_3$, and 10 glucose (equilibrated with 95% O_2 and 5% CO_2, pH 7.4).

Electrophysiology. Slices were transferred to a recording chamber and maintained at 32°C with a continuous bath perfusion of ACSF. Recordings were obtained from thalamic reticular neurons visually identified using differential contrast optics with a Zeiss Axioskop 2 FS microscope (Carl Zeiss) and an infrared video camera. Furthermore, the identity of each neuron was confirmed physiologically through depolarizing voltage-clamp steps to −60 mV that triggered well-clamped transient inward Ca^{2+} (T-type) currents with inactivation time constants of >50 ms (Huguenard and Prince 1992).

Experiments were performed in the whole cell configuration using the patch-clamp technique. The resistance of the electrodes was 2–3 MΩ. During voltage-clamp recordings, the intracellular solution contained (in mM) 130 CsCl, 10 HEPES, 10 EGTA, 2 Mg-ATP, 0.3 Na-GTP, and 5 QX314 (pH = 7.3 adjusted with CsOH, 290 mosm). The liquid junction potential, estimated at +5 mV based on the liquid junction potential calculator in Clampex (Axon Instruments), was not corrected. (−)-Bicuculline methochloride [*R*-(*R**,*S**)]-5-(6,8-dihydro-8-oxofuro[3,4-e]-1,3-benzodioxol-6-yl)-5,6,7,8-tetrahydro-6,6-dimethyl-1,3-dioxolo[4,5-g]isoquinolinium chloride (20 μM), a $GABA_A$ receptor antagonist, was continuously added to the bath perfusion to block fast inhibitory synaptic transmission and isolate excitatory glutamatergic synaptic connections. For some experiments, AMPAR-mediated EPSCs were pharmacologically isolated in the presence of D-(−)-2-amino-5-phosphopentanoic acid (D-AP5; 50 μM) or D-4-[(2E)-3-phosphono-2-propenyl]-2-piperazinecarboxylic acid (SDZ EAA-494 or D-CPP-ene; 5 μM) to block NMDARs, whereas NMDAR-mediated EPSCs were isolated in the presence of the AMPA/kainate receptor antagonist 2,3-dioxo-6-nitro-1,2,3,4-tetrahydrobenzo[f]quinoxaline-7-sulfonamide (NBQX; 10 μM, concentrated stock made up in DMSO with a final concentration of 0.05%). Drugs were delivered using a local perfusion system composed of multiple fine capillaries ending in a common outlet tube, positioned in proximity (~250 μm) to the recorded neuron. The $GABA_A$ receptor blocker, constantly present in the bath, was systematically added in solutions applied by local perfusion as well. All drugs were obtained from Tocris Cookson (Ellisville, MO).

Signals were recorded and amplified with a Multiclamp 700A amplifier (Axon Instruments), sampled, and low-pass filtered at 20 and 2 kHz, respectively. A Digidata 1320 digitizer (Axon Instruments) and PCLAMP9 (Axon Instruments) were used for data acquisition and analysis. Series resistance was constantly monitored, and

data from cells for which this parameter exceeded 15 MΩ or showing changes of >20% of the initial value were rejected. Series resistance was compensated up to 70% of the initial value. In addition, adequacy of the voltage clamp was demonstrated by T-type Ca^{2+} current steady-state inactivation protocols in which peak latencies remained constant after voltage-clamp steps to −55 mV from a range of hyperpolarizing conditioning potentials that evoked currents with constant latency peaks and amplitudes ranging from 20 to 500 pA.

Extracellular stimuli consisting of constant-current pulses, 20–55 μs in duration and 100–450 μA in amplitude, were delivered at low frequency (0.1–0.2 Hz) using a concentric bipolar electrode (tip diameter of 125 μm, CB-ARC75, Frederick Haer, Bowdoinham, ME) for a large majority of experiments (69 of 93 evoked EPSCs). In some cases (24 of 93 cases), we applied current steps more focally through a theta-glass pipette with a very thin tip (diameter: 2–4 μm) and filled with standard ACSF. Type II responses appeared to be more readily evoked by theta-glass stimulating electrodes. We hypothesize that this resulted from a combination of factors, including the more focal stimulus associated with the fine glass electrode and the lower threshold of activation of TC versus CT fibers due to the greater myelination and/or larger fiber diameter of the former (Jones and Powell 1969). Thus, during minimal stimulation, at threshold, the larger metal concentric stimulating electrodes would presumably more readily recruit any TC fiber that was in the recruitable range for this electrode. Data obtained with the two types of electrodes were pooled for analysis. Stimulating electrodes were positioned within the striatum or internal capsule through which both TC and CT fibers pass. Unitary EPSCs mediated by the activation of putative TC or CT single axons were collected using a minimum stimulation protocol while holding the cell at −70 mV (See details in the RESULTS and Fig. 1). To study the properties of short-term plasticity of those synapses, two minimal stimuli were delivered with a 25-ms interval at a frequency of 0.1 Hz.

In another set of experiments, we used a perfusion system to apply glutamate (20–200 μM during 3–5 min) locally in the VB of horizontal slices and specifically activate thalamic relay cells and thalamoreticular synaptic responses in nRt cells. The same protocol was used in TC slices in which the soma and CT connections were preserved (Agmon and Connors 1991; Agmon and Connors 1992), allowing specific glutamate activation of layer 6 pyramidal cells and subsequently corticoreticular inputs.

Data analysis. For each cell, stimulus intensity was adjusted to the minimum value that reliably evoked a single EPSC without failure while holding the membrane potential at −70 mV. The following parameters were systematically analyzed on the average of 10–20 consecutive responses (no failures). We measured the latency of the response defined as the time between the stimulation artifact and the onset of the response. The propagation speed of the stimulated fiber was estimated by dividing the response latency by the distance between stimulating and recording electrodes. The peak amplitude, 10–90% rise time, 90-10% decay time, and half-width of the averaged traces were measured using Clampfit (PCLAMP9, Axon Instruments). The peak to baseline decay phase [$f(t)$] was fitted using the following double-exponential function:

$$f(t) = \left(A_{\text{fast}} e^{-t/\tau\ \text{fast}}\right) + \left(A_{\text{slow}} e^{-t/\tau\ \text{slow}}\right)$$

where A_{fast} and A_{slow} are the fast and slow amplitude components, respectively; τ_{fast} and τ_{slow} are the fast and slow decay time constants, respectively; and t is time. The weighted decay time constant ($\tau_{\text{D,W}}$) was calculated using the following equation:

$$\tau_{\text{D,W}} = \left[\left(A_{\text{fast}}\tau_{\text{fast}}\right) + \left(A_{\text{slow}}\tau_{\text{slow}}\right)\right] / \left(A_{\text{fast}} + A_{\text{slow}}\right)$$

and the percentage of the slow component ($\%_{\text{slow}}$) was computed as follows:

$$\%_{\text{slow}} = \left[A_{\text{slow}} / \left(A_{\text{fast}} + A_{\text{slow}}\right)\right] \times 100$$

When the voltage dependence of the response was tested, approximately three consecutive EPSCs evoked by stimulation while the cell was held at membrane potentials ranging between −70 and +50 mV were averaged, and the resulting trace was used to analyze the AMPA and NMDA components together in control conditions or isolated in the presence of pharmacological blockers. AMPAR-mediated currents were measured at the time of their peak (0.5-ms window) at −70 mV

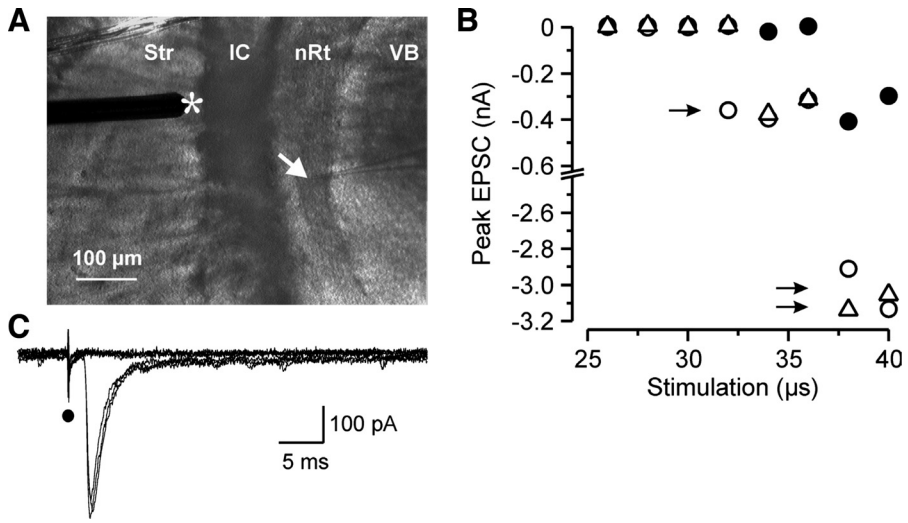

Fig. 1. Minimum stimulation protocol. *A*: photomicrograph of an acute horizontal thalamic slice with the recording pipette (arrow) located in the thalamic reticular nucleus (nRt) and the stimulating electrode (*) positioned in the striatum near the internal capsule (IC) where it activates thalamocortical (TC) and corticothalamic (CT) axonal projections. Str, striatum; VB, ventrobasal complex. *B*: peak amplitude of inward excitatory postsynaptic currents (EPSCs) recorded in a nRt cell at a holding potential of −70 mV during a minimum stimulation paradigm. The intensity of the stimulus was initially fixed slightly above threshold for a 50-μs stimulus and the duration was then progressively stepped from in 2-μs steps from a subthreshold stimulus (25 μs, all failures) until all-or-none responses were triggered. Three consecutive duration series, each represented by a different symbol, of the stimulus were repeated. The minimal stimulation duration was selected as that which was in the middle of the range of durations that evoked threshold responses (as defined as intermixed failures and successes, with the latter being of relatively fixed amplitude, marked with a single arrow). Higher stimulus intensities (longer duration) led to a recruitment of additional fibers and larger responses (double arrows). *C*: current responses from one trial of the minimum stimulation paradigm (26–36-μs durations shown, corresponding only to either failures or minimal responses shown as solid circles in *B*). Note that the onset of the unitary EPSCs occurs at a fixed latency after the stimulation artifact (solid circle) and their time to peak and amplitude remain stable.

and considered to be fully mediated by AMPARs in both control conditions and in the presence of NMDAR antagonists (D-AP5; see Figs. 5*A1* and 6*B1*). The time required for complete decay to baseline of the AMPAR-mediated EPSC component at −70 mV was used to select a time for measurement of the NMDA current in the control condition, starting 60 ms after the stimulation (5 ms window), and therefore excluding contamination by the AMPA/kainate receptor subtype (see Fig. 5*A1*) (Marie et al. 2005; Myme et al. 2003). The complete decay of AMPARs is shown in Fig. 6*B1* in the presence of the NMDAR blocker (D-AP5). In the presence of the AMPAR antagonist (NBQX), NMDAR-mediated currents were measured 15 ms after the stimulation (10-ms window), i.e., close to the peak amplitude of the response (see Fig. 6*B1*). Conductance-voltage (*g-V*) relationships of the AMPA and NMDA components were obtained using the following equation:

$$g = I/\left(V - E_{\text{rev}}\right) \quad (1)$$

where I is the amplitude of the evoked response at holding potential V and E_{rev} is the reversal potential for the activated current. For the AMPA component, E_{rev} (voltage value at $I = 0$) and the conductance (slope) were obtained from a linear fit of the respective current-voltage (*I–V*) curve. For the NMDA component, E_{rev} was measured from the *I–V* relationship, and maximal conductance (g_{max}) was obtained by fitting the *g-V* curve with the following Boltzmann equation using Origin 7.0 (Microcal software, Northampton, MA):

$$g = g_{\text{max}}\left[1 - \left(\left[\text{Mg}^{2+}\right]/\left(\text{K}_{\text{Mg}}e^{(zF\delta V/\text{RT})} + \left[\text{Mg}^{2+}\right]\right)\right)\right] \quad (2)$$

where V is the membrane potential (in V), F is the Faraday constant (9.648×10^4 C/mol), R is the gas constant (8.315 $\text{J}\cdot\text{K}^{-1}\cdot\text{mol}^{-1}$), T is the temperature (32°C/305.2 K), and z is valence (2 for Mg^{2+}). $[Mg^{2+}]$ is the effective concentration of Mg^{2+} (in mM) (Chen and Huang 1992; Kumar and Huguenard 2003; Mayer et al. 1989;). The values of the apparent dissociation constant for Mg^{2+} block at a membrane potential of 0 mV (K_{Mg}; in mM), electrical distance of the Mg^{2+}-binding site in the membrane field (δ), and g_{max} (in nS) were determined by the fit. The potential at which $g/g_{\text{max}} = 0.5$ ($V_{0.5}$) and the Boltzmann slope factor (γ) were calculated as follows:

$$V_{0.5} = \ln\left(\left[\text{Mg}^{2+}\right]/\text{K}_{\text{Mg}}\right)/\left(zF\delta/\text{RT}\right) \quad (3)$$

$$\gamma = \text{RT}/zF\delta \quad (4)$$

Finally, the relative contribution of the NMDA and AMPA components to the response was evaluated with the maximal NMDA conductance ($g_{\text{max NMDA}}$)-to-AMPA conductance (g_{AMPA}) ratio.

Short-term plasticity was estimated by calculating the amplitude and latency of the two responses to paired pulse stimulation and by comparing the values of the first and second EPSCs. This analysis was performed in individual cells on the mean trace obtained from the average of the responses to ~50 successive repetitions of the paired pulse paradigm.

Spontaneously occuring EPSCs (sEPSCs) recorded in the control condition or during glutamate application in the thalamus or cortex were detected and analyzed with locally written software (Wdetecta), a postsynaptic current detection program (http://huguenardlab.stanford.edu/apps/wdetecta). As the specific activation of TC or CT neurons was expected to trigger the generation of sEPSPs, only cells that showed an increase in the frequency of sEPSCs during glutamate application were selected for further analysis. For each cell, the half-width and amplitude of individual sEPSCs were measured, and statistics were then calculated on the total population of events detected over an ~1-min time window of the control, glutamate application, and washout periods (at least 200 events in each condition).

Cluster analysis of unitary EPSCs. To determine whether different types of unitary EPSCs were evoked in the nRt by minimal stimulation, hierarchical cluster analysis was carried out using statistical software (SPSS 12.0, SPSS, Chicago, IL; a custom program written in Origin 7.0, Microcal software), as previously described (Halabisky et al. 2006). Briefly, we used Ward's method and squared Euclidian distances, which determine the "closeness" of individual objects (here, unitary EPSCs) by finding mergers that give the least possible increase of the within-group error sum of squares. Average within-cluster distances were represented on a dendrogram (Fig. 2) and correspond to the squared Euclidian distance between centroids of the merged cluster at each branch point. According to the Thorndike method (Thorndike 1953), large distances between centroids of joined groups at a particular stage relative to other stages suggest there are significant differences between the groups. Multiple discriminant analysis was performed to determine the variables most valuable in predicting the group membership. This analysis consists of a linear combination on variables by assigning weights to each of the parameters to maximize the between-group variance relative to the within-group variance of each discriminant function. The discriminant functions were computed as follows:

$$Z_{jk} = c + W_1X_{1k} + W_2X_{2k} + \ \ldots + W_nX_{nk} \quad (5)$$

where Z_{jk} is the discriminant Z score of discriminant function j for object k, c is the intercept, W_i is the discriminant weight for independent variable i, and X_{ik} is the independent variable i for object k. The number of discriminant functions generated always equals g − 1 (where g is the number of groups being discriminated, two in our case).

Statistical analysis. Results are reported as means ± SE. An independent Student's *t*-test was used to compare EPSCs evoked by minimal electrical stimulation and one-way ANOVA was used to compare EPSCs evoked by glutamate application. Differences were considered significant when $P < 0.05$.

RESULTS

Two populations of synaptic excitatory responses are evoked in the nRt. To study the properties of thalamoreticular and corticoreticular synaptic connections, voltage-clamp recordings were obtained from 93 nRt cells in horizontal slices and EPSCs were evoked by extracellular stimulation applied in the striatum or internal capsule (Fig. 1*A*) that leads to the orthodromic activation of CT axons or antidromic activation of TC axons. The minimal stimulation method has previously been used to study nRt EPSCs in immature mouse slices (Evrard and Ropert 2009), but the properties of excitatory synapses in the rat nRt and in more mature thalamic networks that are able to support thalamic oscillations (Jacobsen et al. 2001) are not known. While holding the membrane potential at −70 mV, putative CT and TC single axon responses were therefore collected with a minimal stimulation paradigm that consists of adjusting the duration of the threshold intensity stimulation until clear all-or-none events occur in ~50% of trials (Fig. 1, *B* and *C*). Failures were likely due to unsuccessful (subthreshold) axon activation as the minimal synaptic response was routinely recovered by slightly increasing the intensity of the stimulus. Once the minimal stimulation parameters were set, it was repetitively applied to the cell, and responses with no significant jitter in latency and a stable time to peak from trial to trial were considered as unitary EPSCs mediated by putative single CT or TC axons. Higher-amplitude stimuli triggered suprathreshold EPSCs, likely mediated by the activation of several fibers (Fig. 1*B*). Multiaxon responses with multiple or unstable latencies were systematically excluded for analysis.

To characterize those minimal electrical excitatory responses and detect whether or not subpopulations of responses

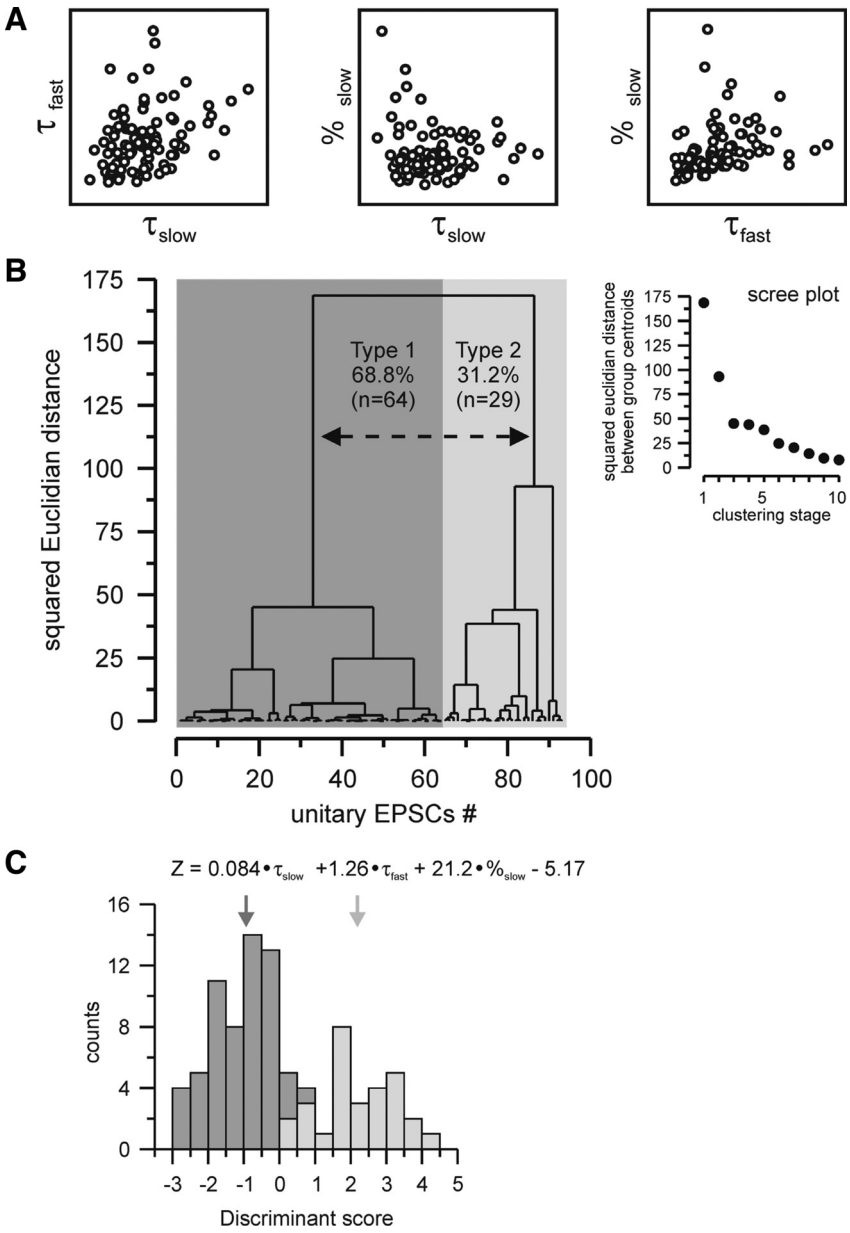

Fig. 2. Classification of minimal EPSCs in nRt cells. *A*: relationship between parameters chosen for hierarchical clustering, with each circle representing an individual EPSC. The slow (τ_{slow}) and fast (τ_{fast}) decay time constants and the contribution of the slow component ($\%_{slow}$) showed little correlation. *B*: dendrogram resulting from hierarchical cluster analysis of the total population of minimal EPSCs. Average within-cluster distance represents the squared Euclidian distance between centroids of the merged cluster at each branch point (the length of vertical lines being proportional to the magnitude of difference). Unitary EPSCs were sorted by closeness along the *x*-axis. *Inset*, scree plot depicting squared Euclidian distances between group centroids during the first 10 clustering stages. Large distances between successive stages are indicative of significant improvement of the classification. Since a such clear division was detected after the first stage but substantially decreased from the second stage; two final groups of synaptic responses were therefore determined, type 1 and type 2, represented by the dashed line on the dendrogram. *C*: multiple discriminant analysis determined the variables most useful in predicting group membership, and the resultant discriminant function is shown. Note that $\%_{slow}$ has the strongest raw discriminating weight. The histogram shows discriminant scores (*Z*) for the responses previously grouped by hierarchical clustering and indicates that the discriminant function accurately predicts group membership: the two types of events are almost completely nonoverlapping in their distributions. Type 1 responses (dark gray bars) had a mean *Z* value of -0.99 ± 0.94 (mean ± SD, $n = 64$, dark gray arrow), whereas type 2 responses (light gray bars) had a mean *Z* value of 2.19 ± 1.12 (mean ± SD, $n = 29$, light gray arrow). There was a small overlap region between *Z* values of 0 and 1; however, no type 2 responses were observed with *Z* scores < 0 and no type 1 responses with *Z* scores >1.

could be distinguished, we performed a cluster analysis on the total population of unitary EPSCs ($n = 93$) evoked in nRt cells. This hierarchical analysis was carried out using τ_{fast}, τ_{slow}, and $\%_{slow}$ of individual EPSCs as variables. These parameters were selected based on their independence (i.e., lack of linear correlation; Fig. 2*A*) and their strong discriminating weight, i.e., the coefficients related to each variable of the discriminant function generated by multiple discriminant analysis (Fig. 2*C*) (Halabisky et al. 2006). While we observed a rise time difference between the different classes of synaptic responses, we found that the rise time was highly correlated with fast decay rates and thus added little discriminatory power to the hierarchical clustering approach. Among the three selected variables, we observed that $\%_{slow}$ had by far the stronger weight, suggesting that the slow component is the most discriminating feature of EPSCs. The resulting classification can be shown in a dendrogram (Fig. 2*B*) in which vertical length represents the degree of dissimilarity between two branches. This analysis provided a clear division in the squared Euclidian distance (Fig. 2*B*, *inset*) at the first clustering stage (distance of ~75) suggesting the existence of two major types of unitary EPSCs evoked in the nRt, representing 68.8% ($n = 64$ of 93, type 1) and 31.2% ($n = 29$ of 93, type 2) of the total population, respectively (Fig. 2*B*). EPSCs from type 1 and type 2 exhibit several distinct properties, as shown in Table 1 and further described below. Subsequent clustering stages after the first step, dissection into two major subclasses, yielded less dramatic reductions in Euclidian distance. While there is a suggestion of subtypes within each of the two major classes, for the sake of parsimony, we did not further consider such subgroups.

Time course and amplitude of the two types of unitary EPSCs evoked in the nRt. We observed that the most discriminating features of the EPSCs between the two populations are related to their overall kinetics, with rise and decay time course being faster in type 1 (Fig. 3*A*). On average (Fig. 3*B1*), the

Table 1. *Properties of evoked unitary EPSCs in nRt cells*

	Type 1	Type 2	*P* Value
Latency, ms**	1.69 ± 0.08 (n = 64)	2.07 ± 0.12 (n = 29)	0.00970
Propagation speed, mm/ms*	0.41 ± 0.02 (n = 63)	0.32 ± 0.02 (n = 27)	0.01210
EPSC amplitude, pA*	473 ± 48 (n = 64)	307 ± 48 (n = 29)	0.03538
EPSC 10–90% rise time, ms***	0.35 ± 0.01 (n = 64)	0.50 ± 0.03 (n = 29)	0.00000
EPSC half-width, ms***	1.14 ± 0.05 (n = 64)	1.99 ± 0.11 (n = 29)	0.00000
EPSC A_{slow}, pA	30 ± 3 (n = 64)	37 ± 6 (n = 29)	0.25652
EPSC A_{fast}, pA*	409 ± 41 (n = 64)	254 ± 41 (n = 29)	0.02415
EPSC $\%_{slow}$***	7.5 ± 0.3 (n = 64)	14.5 ± 1.3 (n = 29)	0.00000
EPSC τ_{slow}, ms***	16.36 ± 0.80 (n = 64)	25.09 ± 2.25 (n = 29)	0.00002
EPSC τ_{fast}, ms***	0.97 ± 0.05 (n = 64)	1.72 ± 0.11 (n = 29)	0.00000
EPSC $\tau_{D,W}$, ms***	2.07 ± 0.09 (n = 64)	4.65 ± 0.25 (n = 29)	0.00000

All data are means ± SE. Control conditions with a single excitatory postsynaptic current (EPSC) at −70 mV are shown. Responses were obtained under conditions isolating ionotropic glutamate EPSCs composed of both non-*N*-methyl-D-aspartate (NMDA)- and NMDA-dependent responses. nRt, thalamic reticular nucleus; A_{fast} and A_{slow}, fast and slow amplitude components, respectively; $\%_{slow}$, percentage of the slow component; τ_{fast} and τ_{slow}, fast and slow decay time constants, respectively; $\tau_{D,W}$, weighted decay time constant. Statistical significance was calculated using an independent Student's *t*-test. *$P < 0.05$; **$P < 0.01$; ***$P < 0.001$.

10–90% rise time was briefer in type 1 responses (0.35 ± 0.01 ms, n = 64) compared with type 2 responses (0.50 ± 0.03 ms, n = 29, $P < 0.001$). Regarding the decay of EPSCs, two components, one slow and one fast, were involved and, therefore, were best fitted with a double-exponential decay function (Fig. 3*B2*). The overall decay, as estimated by $\tau_{D,W}$, was faster in type 1 ($\tau_{D,W}$: 2.07 ± 0.09 ms) versus type 2 ($\tau_{D,W}$: 4.65 ± 0.25 ms, $P < 0.001$), and both the slow and fast components contributed to this difference in decay kinetics (τ_{slow}: 16.36 ± 0.80 ms and τ_{fast}: 0.97 ± 0.05 ms in type 1 vs. τ_{slow}: 25.09 ± 2.25 ms and τ_{fast}: 1.72 ± 0.11 ms in type 2, $P < 0.001$ for both). In contrast, the amplitude of the fast component was larger in type 1 ($P < 0.05$), whereas the amplitudes of the slow component were not different (see Table 1). Interestingly, we observed that the ratio of the amplitude of the slow over the total ($\%_{slow}$; see METHODS) was smaller, 7.5 ± 0.3% for type 1 compared with 14.5 ± 1.3% in type 2 ($P < 0.001$), indicating that the two components contributed to the overall decay with distinct relative weight, the slow one being more prominent in type 2 (Fig. 3*B2*). In addition to these kinetic differences, EPSCs were distinguished by their magnitude, with a larger mean peak amplitude in type 1 (473 ± 48 pA, n = 64) than type 2 (307 ± 48 pA, n = 29, $P < 0.05$).

The two classes of responses had distinct propagation times, with longer latencies for type 2 EPSCs, with an average of 2.07 ± 0.12 ms (n = 29) compared with 1.69 ± 0.08 ms in type 1 (n = 64, $P < 0.01$; Fig. 3*B1*). As synaptic response latency depends on axonal conduction velocity (and presumably, to a lesser extent, on delays associated with synaptic release and the postsynaptic response), we estimated the propagation speed (see METHODS) of single axons that mediate individual EPSCs and found that it was faster for type 1 (0.41 ± 0.02 mm/ms, n = 63) than for type 2 (0.32 ± 0.02 mm/ms, n = 27, $P < 0.05$). This difference likely reflects the activation of different types of axons with distinct diameter and/or amount of myelin, both having a strong influence on axonal conduction, and CT axons develop myelination at later stages than TC axons (Salami et al. 2003; Tsumoto and Suda 1982a; Tsumoto and Suda 1982b). Interestingly, it has been previously shown that CT axons are thinner (Jones and Powell 1969) and have a slower conduction velocity (Gentet and Ulrich 2004; Liu et al. 2001; Swadlow 1990) compared with TC axons. Moreover, larger axons tend to have lower threshold of activation (Ranck Jr. 1975; Swett and Bourassa 1981), and, during our experiments, we observed that the probability to evoke a type 1 response was much higher compared with a type 2 response using the concentric bipolar electrode (74% of type 1 vs. 26% of type 2 EPSCs), whereas the proportion was better balanced if we stimulated via a thin tip theta-glass electrode (54% of type 1 vs. 46% of type 2 EPSCs). This difference in the ability to selectively activate high-threshold type 2 responses with theta-glass stimulating electrodes presumably reflects the more focal nature of the stimuli with this type of electrode with a tip size of ~2 μm compared with the much larger tip size (125 μm) of the concentric electrode.

Specific activation of thalamoreticular and corticoreticular synaptic inputs. Since the nRt receives excitatory inputs from the thalamus and cortex, the type 1 and type 2 responses characterized here using the minimal electrical stimulation paradigm could result from the activation of either TC or CT single fibers. Moreover, large and fast type 1 EPSCs and small and slow type 2 EPSCs displayed properties closely related to those evoked by TC and CT inputs, respectively, reported in previous studies (Beierlein and Connors 2002; Evrard and Ropert 2009; Gentet and Ulrich 2003; Gentet and Ulrich 2004). To provide further support for the identification of type 1 and type 2 EPSCs as originating from TC and CT fibers, we recorded EPSCs evoked in the nRt by the specific activation of thalamic or cortical cells in response to local glutamate applied either in the VB in horizontal thalamic slices or in the cortex in TC slices, respectively, while holding the potential at −70 mV. Glutamate application in both regions (the VB or cortex) induced an increase in EPSC frequency (Fig. 4, *A1* and *A2*). We expected that activation of a given population of presynaptic neurons would result in a relative change in the contribution of CT and TC synaptic responses to the total. For example, if type 1 responses were characteristic of TC inputs, then activation of TC cells should result in a shift in the population of "spontaneous" EPSCs such that the mean response more closely resembles type 1 responses, with larger amplitudes and faster kinetics. Indeed, we found in every case that glutamate application to the thalamus resulted in faster sEPSPs on average (Fig. 4, *B1* and *C*), whereas application to the cortex resulted in slower sEPSCs at the population level

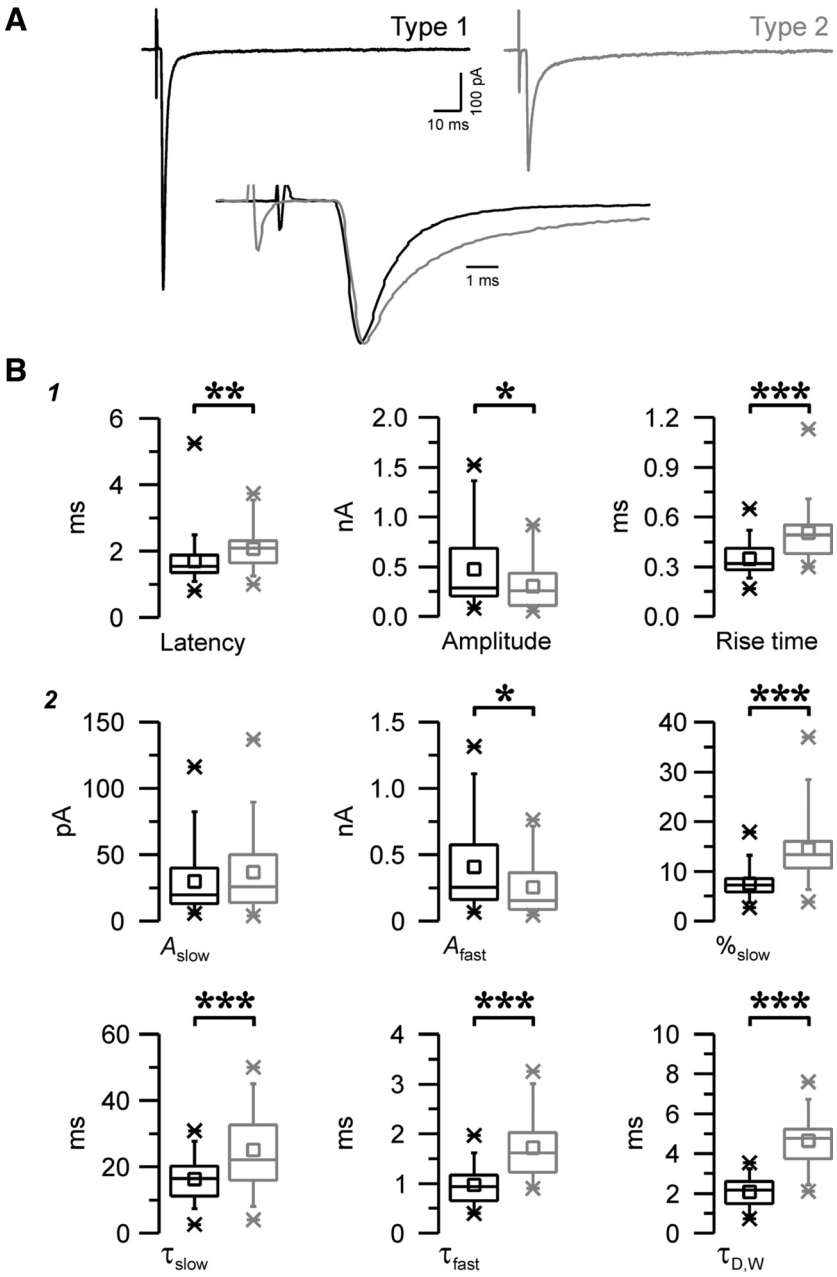

Fig. 3. Distinct properties of the two populations of evoked EPSCs. *A*: examples of a type 1 response (black, *left* trace) and a type 2 response (gray, *right* trace) evoked by minimum stimulation in two nRt cells at a holding potential of −70 mV. Each trace is the average of ~10 EPSCs. *Bottom*, overlay of the *top* traces normalized to the peak and aligned to the onset of the response, showing differences in time course between the two EPSCs. *B*: properties and kinetics of type 1 (black, $n = 64$) and type 2 (gray, $n = 29$) evoked EPSCs. Parameters were obtained either from the statistics of the averaged traces (*1*) or extracted from the fitted double-exponential decay functions (*2*). Note that overall type 1 EPSCs were larger (amplitude) and faster [smaller rise time, τ_{fast}, τ_{slow}, and weighted decay time constant ($\tau_{D,W}$)] and the contribution of the slow component ($\%_{slow}$) was more prominent in type 2. A_{fast} and A_{slow} are the fast and slow amplitude components, respectively. $^{*}P < 0.05$; $^{**}P < 0.01$; $^{***}P < 0.001$.

(Fig. 4, *B2* and *C*), and these changes were generally reversible upon glutamate washout. Similar trends were seen with sEPSC amplitude, i.e., larger and smaller sEPSCs during thalamic and cortex activation, respectively (Fig. 4*B*). Although the differences we observed were small on average (thalamic glutamate: half-width of 1.35 ± 0.08 ms in control vs. 1.29 ± 0.08 ms during glutamate vs. 1.38 ± 0.07 ms after washout, $n = 4$; cortical glutamate: half-width of 1.42 ± 0.08 ms in control vs. 1.49 ± 0.08 ms during glutamate vs. 1.47 ± 0.09 ms after washout, $n = 6$; Fig. 4*C*), these results reinforced the hypothesis that type 1 and type 2 responses are likely related to the activation of thalamoreticular and corticoreticular inputs, respectively.

At least part of the functional differences we described here between the two populations of EPSCs could be due to the activation of distinct subtypes of synaptic receptors (Arrigoni and Greene 2004; Hollmann and Heinemann 1994; Kumar and Huguenard 2003). Therefore, to address this question, we next investigated whether or not these two populations of minimal responses exhibited differences in voltage dependence and/or related properties such as sensitivity to voltage-dependent blockade of NMDAR by Mg^{2+}.

Voltage dependence properties and relative contribution of AMPARs and NMDARs. To determine the *I–V* relation of unitary EPSCs in the two populations, we obtained minimal synaptic responses while holding the membrane potential at various values in the range of −70 to +50 mV using 10-mV increments. The examples shown in Fig. 5*A1* show that both type 1 and type 2 EPSCs were composed of an initial peak with a fast time course followed by a late slow component with distinct voltage dependence, which we analyzed separately (see METHODS). As shown in the *I–V* plots (Fig. 5*A2*), the early peak of the EPSCs demonstrated a linear *I–V* slope, with its amplitude being proportional to the driving force, i.e., the

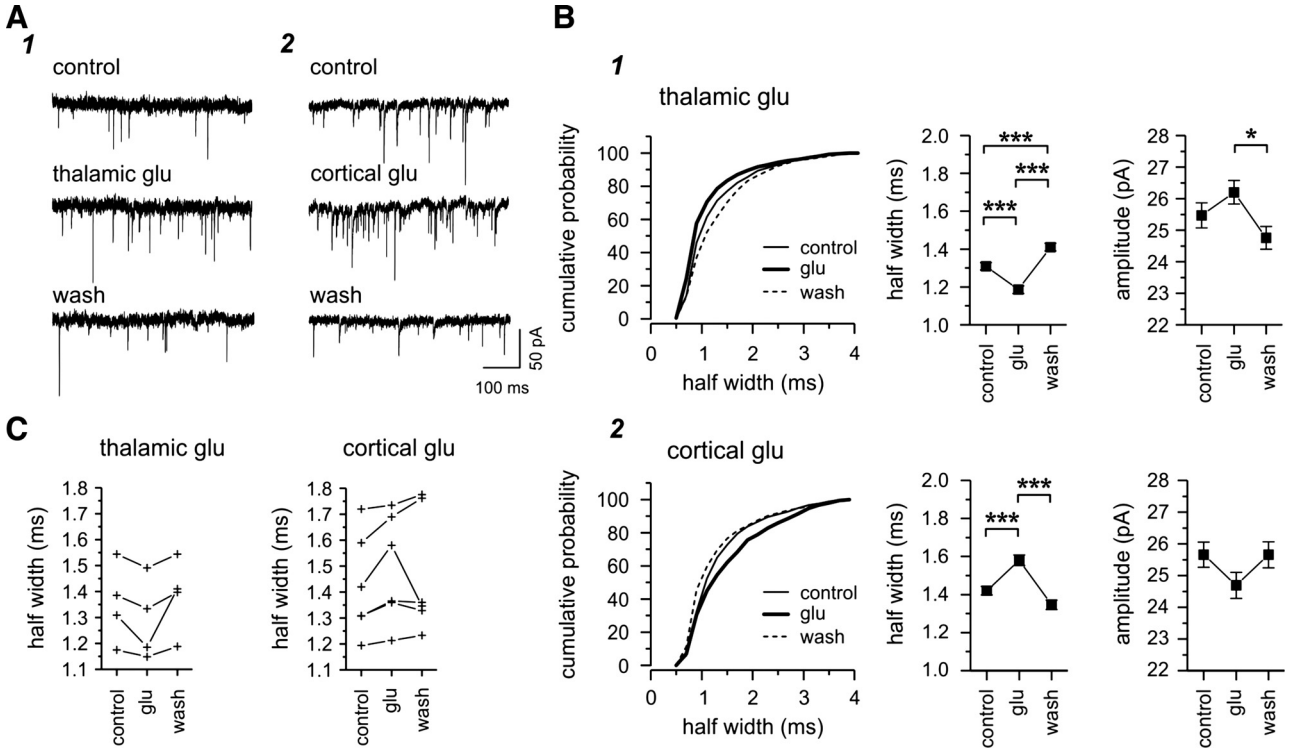

Fig. 4. Glutamate (Glu) activation of thalamic or cortical neurons. *A*: examples of spontaneously occurring EPSCs recorded in two different nRt cells before (control), during (thalamic or cortical glutamate), and after glutamate application (wash) in the thalamus (*1*; 25 μM glutamate) or cortex (*2*; 200 μM glutamate) in horizontal or TC slices, respectively. Glutamate activation resulted in an increased number of EPSCs. *B*: subsequent analysis of all EPSCs recorded in the same cells and conditions as in *A*. Equivalent periods of recording were analyzed in each condition (1 min for the VB and 30 s for the cortex). The cumulative probability curve for half-width of all EPSCs showed a leftward shift (i.e more fast events) during glutamate activation (thick curve) in the thalamus (*B1*) but a right shift (i.e., more slow events) during cortical glutamate (*B2*). These opposite changes occurring during thalamic or cortical glutamate are also reflected in the mean half-width as well as amplitude (chevron plots) with an increased amplitude during glutamate activation in the thalamus but a decreased amplitude during glutamate application in the cortex, although the differences were not statistically different. *C*: glutamate-induced changes for the total population of nRt cells. Each line represents a nRt cell. In each case, thalamic application (*left*) resulted in a decreased mean half-width, whereas cortical application (*right*) resulted in an increased mean half-width. In most cases, the changes were reversible. Overall, the majority of fast and large events were triggered by glutamate activation of thalamic neurons, and these properties were reminiscent of type 1 evoked EPSCs. In contrast, occurrence of slow and small events seemed to predominate during the activation of cortical neurons, resembling the properties of type 2 EPSCs. $^*P < 0.05$; $^{***}P < 0.001$.

difference between membrane potential and the EPSC reversal potential of 0 mV. In contrast, the amplitude of the late EPSC showed a nonlinear dependence on membrane voltage, with a region of negative slope, and it decayed gradually over hundreds of milliseconds. Both early and late components reversed close to the reversal potential of ionotropic glutamate receptors (~0 mV). Thus, the early peak current has characteristics of AMPAR-mediated currents in terms of the rapid time course and voltage independence, whereas the slow component has properties consistent with NMDAR-mediated currents, such as a slower time course and, in particular, rectification known to result from voltage-dependent Mg^{2+} block of the NMDAR (Nowak et al. 1984). These data suggest that both AMPA- and NMDAR-mediated currents contribute to unitary EPSCs in the two populations.

The magnitude of voltage-independent AMPA conductance was extracted from the *I–V* curve as the slope of the linear regression (Fig. 5*A2*). In contrast, NMDA conductance was first calculated based on the amplitude of the current at each voltage (with a reversal potential of 0 mV), and the resultant *g–V* curve was then fitted using a Boltzmann function. The value of the fitted curve at saturation was considered as the maximum NMDA conductance (Fig. 5*A3*; see METHODS). On average (Fig. 5*B* and Table 2), AMPA conductance (g_{AMPA}) was larger in type 1 EPSCs (6.94 ± 0.75 nS, $n = 49$) compared with type 2 EPSCs (4.13 ± 0.94 nS, $n = 17$, $P < 0.05$), whereas maximal NMDA conductance ($g_{max\ NMDA}$) did not show significant differences (3.58 ± 0.37 nS, $n = 48$, in type 1 vs. 3.68 ± 0.75 nS, $n = 17$, in type 2). However, to estimate the relative contribution of the NMDA and AMPA components to total EPSC, we calculated $g_{max\ NMDA}/g_{AMPA}$. Interestingly, we observed that the ratio was smaller in type 1 (0.57 ± 0.03, $n = 48$) than in type 2 (0.99 ± 0.09, $n = 17$) synapses ($P < 0.001$). This difference is also well illustrated in Fig. 5*A3*, in which maximum value of the type 1 nonlinear NMDA *g-V* curve ($g_{max\ NMDA}$) was much smaller than that of the more linear AMPA *g-V* curve, whereas type 2 responses had comparable g_{max} values for NMDA- and AMPAR-mediated components. Thus, the slower NMDA component was more prominent in type 2 EPSCs.

The voltage-dependent properties of NMDA conductance were further investigated from the fit of the *g-V* curve of individual EPSCs (Fig. 5, *A3*, *B*, and *C*, and Table 2). The mean value of the voltage at which 50% of the conductance was activated ($V_{0.5}$) was more depolarized in type 1 (−0.92 ± 1.08 mV, $n = 48$) compared with type 2 EPSCs (−7.92 ± 2.02 mV, $n = 17$, $P < 0.01$), whereas the slope, quantified as slope factor γ (see METHODS), was not significantly different (γ: 15.5

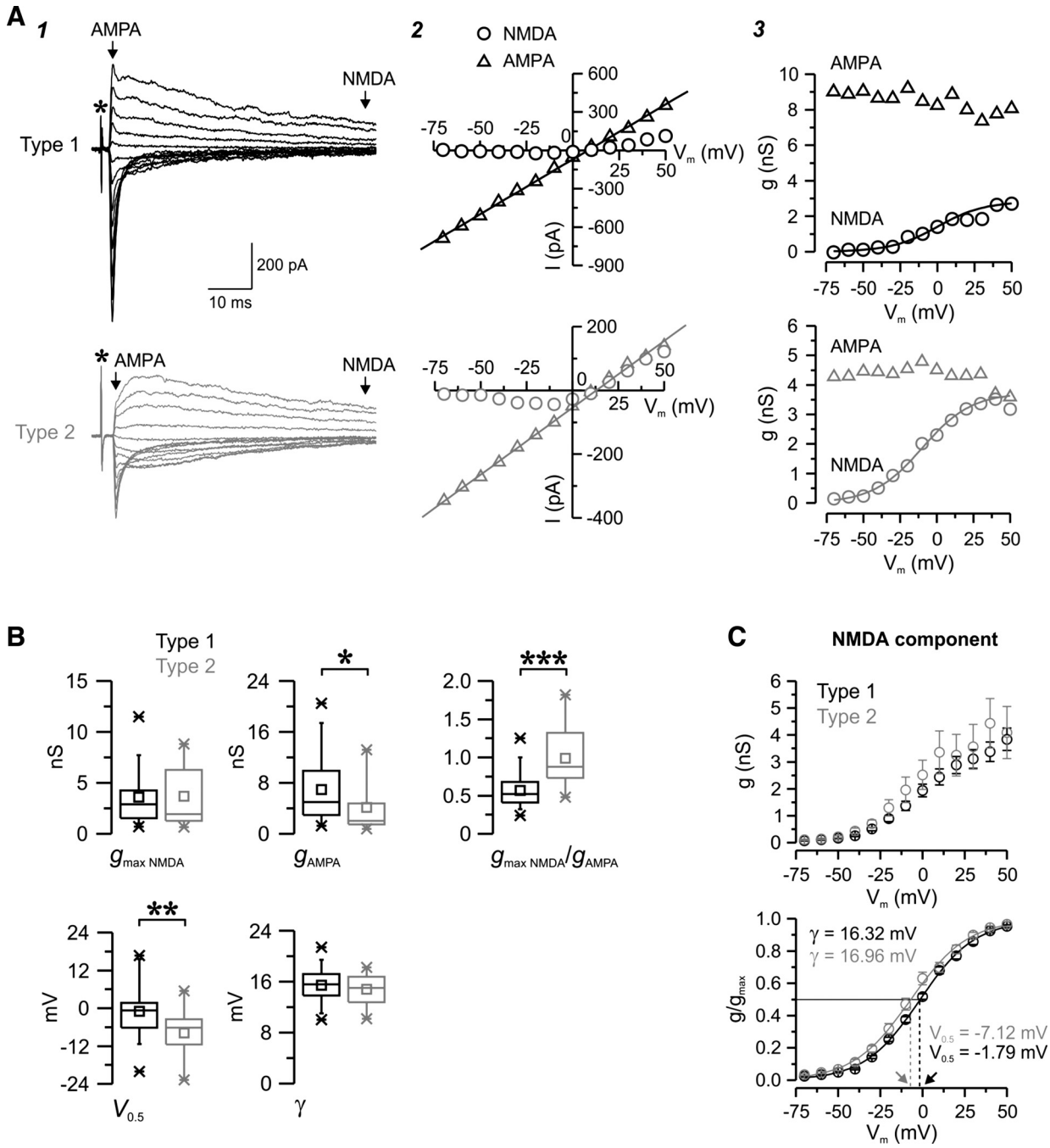

Fig. 5. Voltage dependence of the two populations of evoked EPSCs. *A*: examples of unitary type 1 (black) and type 2 (gray) EPSCs triggered by minimum stimulation in nRt cells in control conditions while the membrane potential was held at different levels (*1*) together with the corresponding current-voltage (*I–V*; *2*) and conductance-voltage (*g–V*; *3*) relationship. Each trace is the average of two (type 1) or three (type 2) trials. *Time of stimulation (*A1*). The putative α-amino-3-hydroxy-5-methyl-4-isoxazolepropionic acid (AMPA; triangles) and *N*-methyl-D-aspartate (NMDA; circles) currents were measured at the times indicated by the arrows in *A1*. AMPA *I–V* and NMDA *g–V* curves were fitted with a linear regression (line in *A2*) and a Boltzmann function (line in *A3*), respectively, and parameters were extracted from fits. For these prototypical responses, the following fitted curve parameters were obtained: maximal NMDA conductance ($g_{max\ NMDA}$; in nS), 2.83 for type 1 vs. 3.73 for type 2; apparent dissociation constant for Mg^{2+} block at a membrane potential of 0 mV (K_{Mg}), 0.7 mM for type 1 vs. 1.3 mM for type 2; electrical distance of the Mg^{2+}-binding site in the membrane field (δ), 0.85 for type 1 vs. 0.79 for type 2; voltage at which 50% of the conductance was activated ($V_{0.5}$), 0.09 mV for type 1 vs. −9.88 for type 2; slope factor (γ), 15.6 mV for type 1 vs. 16.7 mV for type 2; AMPA conductance (g_{AMPA}), 8.6 nS for type 1 vs. 4.2 nS for type 2; and $g_{max\ NMDA}/g_{AMPA}$, 0.33 for type 1 vs. 0.89 for type 2. *B*: population statistics for type 1 (black, $n = 48$) and type 2 (gray, $n = 17$) EPSCs. Note the more prominent contribution of the NMDA component in type 2, reflected by a higher ratio between $g_{max\ NMDA}$ and g_{AMPA}. $V_{0.5}$ was more hyperpolarized in type 2, suggesting reduced sensitivity to Mg^{2+} block. *$P < 0.05$; **$P < 0.01$; ***$P < 0.001$. *C*: population data for NMDA. Averaged (*top* graph) and normalized (*bottom* graph) NMDA *g-V* curves of type 1 (black) and type 2 (gray) responses are shown. Fitted curves (curved line) had similar γ values but distinct $V_{0.5}$ values (see METHODS), thus confirming the differences in sensitivity to voltage-dependent Mg^{2+} block between the two types. Arrows indicate differences in $V_{0.5}$ values between type 1 and type 2 EPSCs, i.e., the voltage (straight dotted lines) at which 50% of the maximum conductance is activated (straight black line).

Table 2. *Voltage-dependent properties of putative AMPA (short latency) and NMDA (long latency) components of evoked composite nRt EPSCs*

	Type 1	Type 2	*P* Value
g_{NMDA}			
$g_{max\ NMDA}$, nS	3.58 ± 0.37 (n = 48)	3.68 ± 0.75 (n = 17)	0.89918
K_{Mg}, mM**	0.93 ± 0.08 (n = 48)	1.64 ± 0.28 (n = 17)	0.00149
δ	0.87 ± 0.02 (n = 48)	0.92 ± 0.04 (n = 17)	0.34819
$V_{0.5}$, mV**	−0.92 ± 1.08 (n = 48)	−7.92 ± 2.02 (n = 17)	0.00197
γ, mV	15.5 ± 0.4 (n = 48)	14.8 ± 0.6 (n = 17)	0.33537
g_{AMPA}			
g_{AMPA}, nS*	6.94 ± 0.75 (n = 49)	4.13 ± 0.94 (n = 17)	0.04813
$g_{max\ NMDA}/g_{AMPA}$			
$g_{max\ NMDA}/g_{AMPA}$***	0.57 ± 0.03 (n = 48)	0.99 ± 0.09 (n = 17)	0.00000

All data are means ± SE. Control conditions are shown. g_{NMDA}, NMDA conductance; $g_{max\ NMDA}$, maximal conductance of NMDA; K_{Mg}, apparent dissociation constant for Mg^{2+} block at a membrane potential of 0 mV; δ, electrical distance of the Mg^{2+}-binding site in the membrane field; $V_{0.5}$, voltage at which 50% of the conductance was activated; γ, slope factor; g_{AMPA}, α-amino-3-hydroxy-5-methyl-4-isoxazolepropionic acid (AMPA) conductance. Statistical significance was calculated using an independent Student's *t*-test. *$P < 0.05$; **$P < 0.01$; ***$P < 0.001$.

± 0.4 mV in type 1, n = 48, and 14.8 ± 0.6 mV in type 2, n = 17; Fig. 5*B*). This result was confirmed when individual *g-V* curves were normalized to their maximum (g/g_{max}) and then averaged for the total type 1 and type 2 population, and the resulting mean curves were subsequently fitted (Fig. 5*C*). Indeed, we observed a leftward shift (5.7-mV more hyperpolarized voltage) of the mean normalized *g-V* curve of type 2 compared with type 1 ($V_{0.5}$: −1.79 mV in type 1 and −7.12 mV in type 2) with no change in the slope (γ: 16.32 mV in type 1 and 16.96 mV in type 2). These data suggest that the voltage dependence of NMDA conductance was comparable in the two populations (similar slope) but the sensitivity to voltage-dependent blockade of NMDAR by Mg^{2+} ($V_{0.5}$ more hyperpolarized) was reduced in the type 2 population. Therefore, at resting potential, the contribution of the NMDA component to the total current was more prominent in the type 2 population. These results were in accordance with a greater NMDA contribution and hence slower decay of type 2 single EPSCs triggered at −70 mV (Fig. 3). Moreover, the apparent dissociation constant for the Mg^{2+} block at 0 mV (K_{Mg}) reflects the affinity of Mg^{2+} for its binding site within the NMDAR. Interestingly, we observed that, on average (Fig. 5*B* and Table 2), the K_{Mg} value was smaller (i.e., more effective at a given membrane voltage and Mg^{2+}) in type 1 (0.93 ± 0.08 mM, n = 48) than in type 2 EPSCs (1.64 ± 0.28 mM, n = 17, $P < 0.01$). This suggests that the NMDARs mediating the slow component of EPSCs in type 1 synapses would require a lower concentration of Mg^{2+} to reach the same degree of blockade at a given membrane voltage. Finally, the estimated electrical location of the Mg^{2+}-binding site in the membrane field (δ; see the Boltzmann equation in METHODS) showed no significant difference between the two populations (0.87 ± 0.02 in type 1 vs. 0.92 ± 0.04 in type 2), indicating that differences in Mg^{2+} block are accounted for simply on the basis of different affinities of Mg^{2+} for the binding site mediating channel block.

Pharmacology of unitary evoked EPSCs. The properties of AMPA- and NMDAR-mediated currents and their relative contribution to total EPSCs were further investigated by recording pharmacologically isolated AMPAR- and NMDAR-mediated unitary EPSCs. The AMPA and NMDA components were isolated by the application of the NMDAR antagonists D-AP5 or D-CPP-ene and the AMPA/kainate receptor antagonist NBQX, respectively. At a holding potential of −70 mV, D-AP5 blocked a portion of the late slow current but did not antagonize the prominent early fast current (not shown). Interestingly, this indicates that NMDARs were activated and further supports the incomplete blockade of NMDARs by Mg^{2+} at membrane potentials near rest, as suggested by the *g-V* analysis shown in Fig. 5. Additional application of the AMPAR antagonist NBQX completely abolished this AP5-insensitive current, both early fast and later slow components, indicating that unitary EPSCs triggered by stimulation of either type 1 or type 2 (putative thalamoreticular and corticoreticular, respectively) single axons resulted in glutamate release at synapses containing both AMPA and NMDAR. In particular, the blockade of the majority of the slow EPSC component by D-AP5 or D-CPPene suggests a minimal involvement of slow kainate receptors at these synapses (Fig. 6*B*). The combination of successive applications of AP5 + NBQX or NBQX + AP5 was tested on 18 cells from type 1 (n = 12) or type 2 (n = 6; data not shown). We then analyzed the properties of these pharmacologically isolated AMPA (Fig. 6) and NMDA (Fig. 7) components in the two populations of EPSCs determined by cluster analysis in control conditions, and the results are shown in Table 3.

In the presence of the NMDAR antagonist, AMPAR-mediated EPSCs evoked at −70 mV remained larger and faster in type 1 compared with type 2 (Fig. 6*A*). Indeed, as shown in the example in Fig. 6*A1* where normalized traces were overlaid (Fig. 6*A1*, *bottom*), the peak of AMPAR-mediated EPSCs occurred later (was delayed) and the current decayed more slowly in type 2. On average (Fig. 6*A2* and Table 3), the 10–90% rise time was 0.39 ± 0.02 ms in type 1 (n = 8) compared with 0.51 ± 0.04 ms in type 2 (n = 7, $P < 0.05$). As for control EPSCs, the decay of the AMPAR-mediated current was best fitted using a double-exponential function. On average, the weighted decay time constant was significantly slower in type 2 (2.74 ± 0.25 ms, n = 7) than in type 1 (1.58 ± 0.26 ms, n = 8, $P < 0.01$). The slow and fast components contributed to the decay kinetics of the AMPA current, with both time constants tending to be slower in type 2 (τ_{slow}: 5.95 ± 0.96 ms and τ_{fast}: 1.14 ± 0.20 ms in type 1 vs. τ_{slow}: 15.70 ± 3.53 ms and τ_{fast}: 1.71 ± 0.17 ms in type 2), but only the slow components were significantly different ($P < 0.05$). However, in contrast to the control condition, the contribution of the slow component to the total AMPAR-mediated current was similar in the two populations of EPSCs ($\%_{slow}$: 10.2 ± 2.3 in type 1 vs. 10.0 ± 2.4 in type 2), reinforcing the hypothesis that the prominent slow component observed in the type 2 population in the control condition was probably not mediated by AMPARs. Finally, the mean amplitude of AMPAR-mediated EPSCs tended to be larger for type 1 (491 ± 102 pA, n = 8) than type 2 (300 ± 56 pA, n = 7), although the difference was not significant, likely due to the small number of samples. As shown in the *I–V* curve examples (Fig. 6*B1*), for the two populations of EPSCs, NMDAR antagonists abolished the slow voltage-dependent current activated mainly at depolarized potentials, whereas the early fast current prominent at hyperpolarized potentials remained and was linearly related to voltage. Note that the decay was slower in the type 2 population at

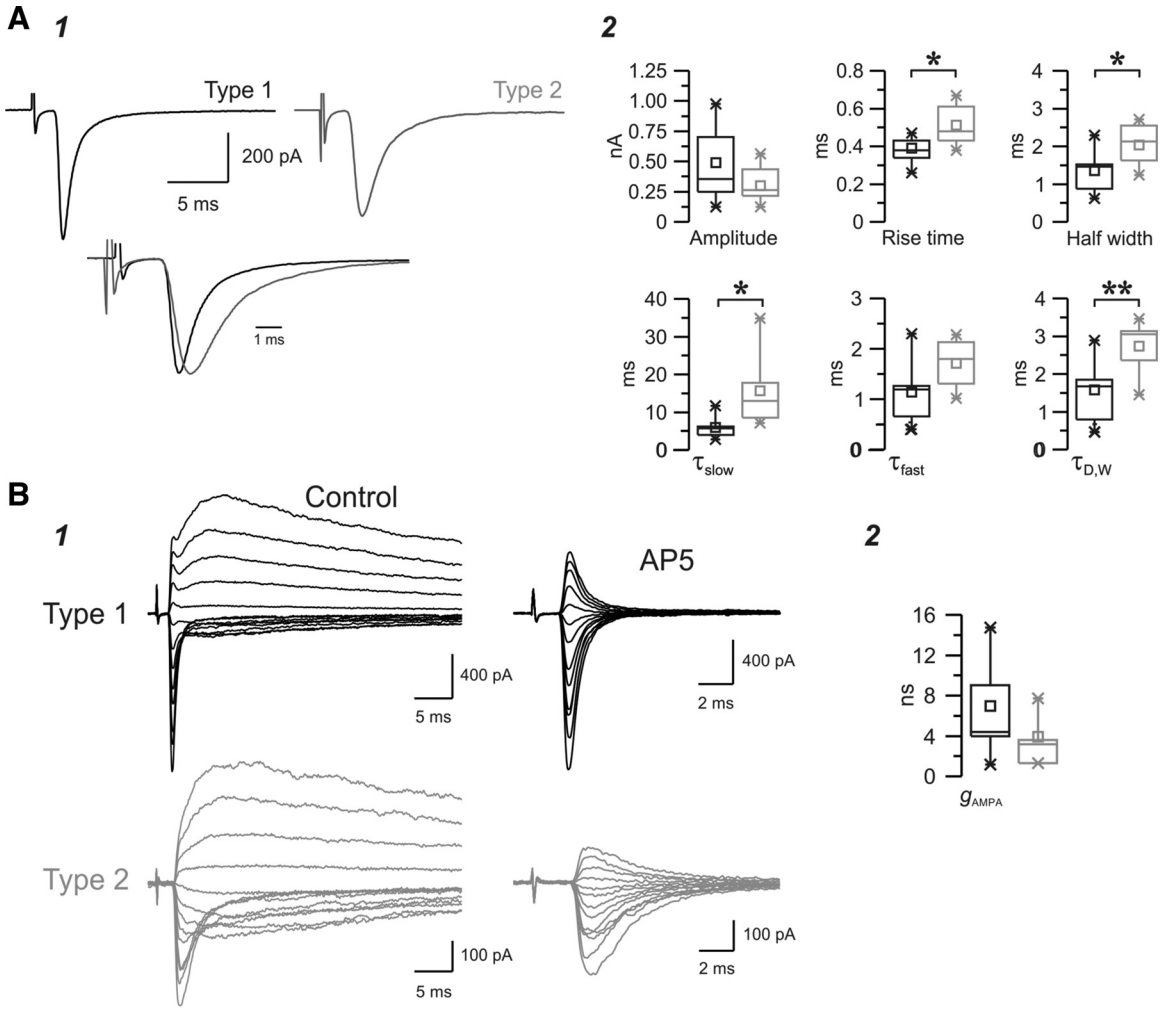

Fig. 6. Properties of isolated AMPA receptor (AMPAR)-mediated EPSCs evoked in the nRt. *A*: pharmacologically isolated type 1 (black) and type 2 (gray) AMPAR-mediated EPSCs recorded in representative nRt cells in the presence of the NMDAR antagonist D-(−)-2-amino-5-phosphopentanoic acid (D-AP5) at a holding potential of −70 mV. As shown in the example (*A1*; each trace is the average of ~10 EPSCs), type 1 responses tended to be larger and faster. The *bottom* overlay of the two traces, normalized to the peak and aligned to the onset of the response, highlights the slower rise and decay time course of EPSCs in type 2. These strong differences in the kinetics and amplitude of the total population of AMPAR-mediated responses were apparent in the population statistics (*A2*) and confirmed the slower rise and decay time, longer half-width, and smaller amplitude of the EPSCs in type 2 ($n = 7$) compared with type 1 ($n = 8$). *B*: example of evoked EPSCs obtained at a range of potentials between −75 and +50 mV using 10-mV voltage increments (*1*) for a type 1 response (*top* traces) and a type 2 response (*bottom* traces) in two nRt cells under control conditions (*left* traces) and during the application of D-AP5 (traces expanded along the *x*-axis), which blocks the late and slow component of the response (*middle* traces), leaving only the fast early component of the EPSC. Each trace is the average of two (type 2) or three (type 1) trials. Mean AMPA conductance tended to be larger in type 1 ($n = 6$) compared with type 2 ($n = 4$), although the differences were not significantly different (*B2*). $^*P < 0.05$; $^{**}P < 0.01$.

all membrane potentials tested. As in the control condition, the pharmacologically isolated AMPA component was linearly related to voltage and reversed at ~0 mV (data not shown). Additional application of the AMPAR antagonist completely abolished the current ($n = 9$ cells; data not shown). The mean isolated AMPA conductance tended to be larger (6.96 ± 1.96 nS, $n = 6$) for type 1 than Type 2 (3.95 ± 1.35 nS, $n = 4$), but the differences were not significant (Fig. 6*B2* and Table 3). Because we did not observe differences between the effect of D-AP5 and D-CPP-ene, data were pooled.

The properties of the NMDA component of EPSCs were studied while the cells were held at +30 mV in the presence of the AMPAR antagonist NBQX. As shown in Fig. 7*A*, the magnitude and kinetics of the isolated NMDAR-mediated current were similar in the two populations of EPSCs. Indeed, on average, the difference between the two types of NMDAR-mediated EPSCs in peak amplitude (130 ± 25 pA, $n = 16$, in type 1 vs. 134 ± 78 pA, $n = 4$, in type 2), 10–90% rise time (4.01 ± 0.55 ms in type 1 vs. 4.66 ± 1.02 ms in type 2), and half-width (35.97 ± 2.13 ms in type 1 vs. 41.90 ± 6.80 ms in type 2) were not significant (Fig. 7*B* and Table 3). The decay times of EPSCs were similar as well (see Table 3). EPSCs were also evoked at different holding potentials to study the voltage-dependent properties of the isolated NMDA component. As in the control condition, the *I–V* curve in the presence of NBQX was nonlinear and the reversal potential was close to 0 mV (data not shown). On average (see Table 3), the properties of pharmacologically isolated NMDA EPSCs were similar to those of the slow-latency NMDA component measured on the composite response in control conditions (Table 2 vs. Table 3). In particular, the differences in voltage dependence and sensitivity to Mg^{2+} block were consistent in type 2 ($V_{0.5}$: −12.57 ±

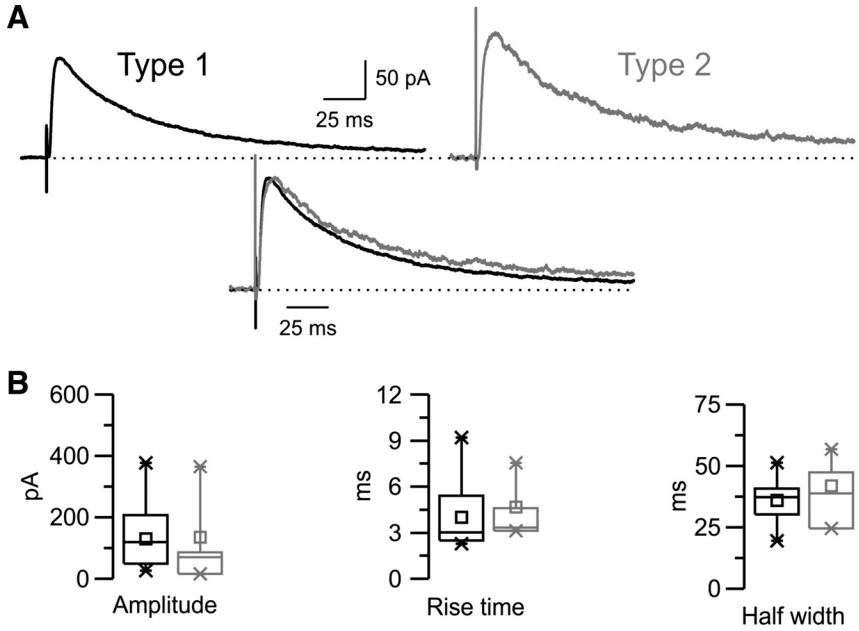

Fig. 7. Properties of isolated NMDA receptor (NMDAR)-mediated EPSCs evoked in the nRt. *A*: pharmacologically isolated NMDAR-mediated EPSCs evoked in the presence of the AMPAR antagonist 2,3-dioxo-6-nitro-1,2,3,4-tetrahydrobenzo[f]quinoxaline-7-sulfonamide (NBQX) while the cell was held at +30 mV (dotted line). Type 1 (black) and type 2 (gray) traces were plotted separately (*top* traces) or overlapped after normalization to the peak and alignment to the onset of the responses (*bottom* traces). Each trace is the average of responses recorded in several cells for type 1 ($n = 15$) or type 2 ($n = 4$) responses, which, when overlapped, revealed little difference in the NMDA response. *B*: corresponding box charts showing no significant difference in amplitude or kinetics between the two groups.

2.07 mV and K_{Mg}: 1.69 ± 0.23 mM, $n = 4$) compared with type 1 ($V_{0.5}$: −8.56 ± 1.98 mV and K_{Mg}: 1.37 ± 0.15 mM, $n = 16$) responses, although the differences were not significant, presumably owing to the small sample size. Nevertheless, these results support the general conclusions regarding the differences in Mg^{2+} blockade of the NMDARs underlying type 2 versus type 1 responses. Moreover, as in the control condition, the magnitude of the NMDAR-mediated current and its dependence to voltage were similar in the two groups, as suggested by the mean values of maximal NMDA conductance and the slope of the fitted curve, respectively ($g_{max\ NMDA}$ 5.49 ± 0.90 nS and γ: 16.01 ± 0.30 mV in type 1; $g_{max\ NMDA}$ 5.46 ± 2.73 nS and γ: 14.97 ± 0.46 mV in type 2).

Short-term plasticity properties. We also investigated the short-term plasticity of the two types of responses. This plasticity could arise from a number of mechanisms, including

Table 3. *Properties of pharmacologically isolated AMPA receptor- and NMDA receptor-mediated EPSCs*

	Type 1	Type 2	*P* Value
	With NMDA receptor antagonist		
AMPA at −70 mV			
AMPA amplitude, pA	491 ± 102 ($n = 8$)	300 ± 56 ($n = 7$)	0.14048
AMPA 10–90% rise time, ms*	0.39 ± 0.02 ($n = 8$)	0.51 ± 0.04 ($n = 7$)	0.02029
AMPA half-width, ms*	1.36 ± 0.18 ($n = 8$)	2.04 ± 0.20 ($n = 7$)	0.02528
AMPA 90–10% decay time, ms*	3.26 ± 0.53 ($n = 8$)	5.46 ± 0.67 ($n = 7$)	0.02209
AMPA A_{slow}, pA	48 ± 18 ($n = 8$)	24 ± 5 ($n = 7$)	0.23807
AMPA A_{fast}, pA	403 ± 82 ($n = 8$)	255 ± 51 ($n = 7$)	0.16371
AMPA $\%_{slow}$	10.2 ± 2.3 ($n = 8$)	10.0 ± 2.4 ($n = 7$)	0.95168
AMPA τ_{slow}, ms*	5.95 ± 0.96 ($n = 8$)	15.70 ± 3.53 ($n = 7$)	0.01414
AMPA τ_{fast}, ms	1.14 ± 0.20 ($n = 8$)	1.71 ± 0.17 ($n = 7$)	0.05516
AMPA $\tau_{D,W}$, ms**	1.58 ± 0.26 ($n = 8$)	2.74 ± 0.25 ($n = 7$)	0.00769
g_{AMPA}			
g_{AMPA} (nS)	6.96 ± 1.96 ($n = 6$)	3.95 ± 1.35 ($n = 4$)	0.29410
	With AMPA receptor antagonist		
NMDA at +30 mV			
NMDA amplitude, pA	130 ± 25 ($n = 15$)	134 ± 78 ($n = 4$)	0.94232
NMDA 10–90% rise time, ms	4.01 ± 0.55 ($n = 15$)	4.66 ± 1.02 ($n = 4$)	0.59376
NMDA half-width, ms	35.97 ± 2.13 ($n = 15$)	41.90 ± 6.80 ($n = 4$)	0.27939
NMDA 90–10% decay time, ms	136.35 ± 7.79 ($n = 15$)	169.10 ± 34.21 ($n = 4$)	0.16093
NMDA $\tau_{D,W}$, ms	75.65 ± 3.77 ($n = 15$)	79.29 ± 14.12 ($n = 4$)	0.72018
g_{NMDA}			
$g_{max\ NMDA}$, nS	5.49 ± 0.90 ($n = 16$)	5.46 ± 2.73 ($n = 4$)	0.98914
K_{Mg}, mM	1.37 ± 0.15 ($n = 16$)	1.69 ± 0.23 ($n = 4$)	0.32608
δ	0.82 ± 0.01 ($n = 16$)	0.88 ± 0.03 ($n = 4$)	0.09857
$V_{0.5}$, mV	−8.56 ± 1.98 ($n = 16$)	−12.57 ± 2.07 ($n = 4$)	0.34702
γ, mV	16.01 ± 0.30 ($n = 16$)	14.97 ± 0.46 ($n = 4$)	0.12181

All data are means ± SE. Control conditions are shown. Statistical significance was calculated using an independent Student's *t*-test. *$P < 0.05$; **$P < 0.01$; ***$P < 0.001$.

changes in axonal conduction and/or in the synaptic machinery, which influence the latency and amplitude of the synaptic responses, respectively. We therefore tested responses to a pair of minimal stimuli applied with a 25-ms interval (40 Hz) in 25 nRt cells while holding the membrane potential at −70 mV. We repeated the pair of stimuli ~50 times in each cell and analyzed the resulting average trace. Axon excitability can change during repetitive extracellular activation. Axons that exhibit an increase in conduction velocity and a decrease in threshold are supernormal (Beierlein and Connors 2002; Swadlow 1974; Swadlow 1990), whereas those exhibiting a decrease of conduction velocity and an increase in threshold of activation are subnormal. Thus, supernormality is associated with a decreased latency between the stimulus and response for the second pulse compared with the first pulse.

Thus, we compared the latency of the response to the first pulse (EPSC1) and second pulse (EPSC2) to evaluate the normality properties of our type 1 and type 2 responses (Fig. 8, *A* and *B*). We also investigated whether the synaptic responses displayed short-term depression or facilitation, i.e., decrease or increase in amplitude, respectively (Fig. 8, *A* and *C*). An example of the paired pulse paradigm in the type 1 and type 2 groups is shown in Fig. 8*A*, with the responses to EPSC1 and EPSC2 aligned to the time of stimulation (Fig. 8*A*, *bottom*) to show short-term plasticity changes. When we compared EPSC1 and EPSC2 in individual cells, the large majority of the type 1 responses ($n = 18$) displayed a consistent increase in latency (1.53 ± 0.09 ms for EPSC1 vs. 1.64 ± 0.10 ms for EPSC2; Fig. 8*B*, *left*) and decrease in amplitude (Fig. 8*C*, *left*) of EPSC2 (−0.40 ± 0.08 nA) compared with EPSC1 (−0.46 ± 0.08 nA), indicative of highly significant subnormal conduction ($P < 0.001$) and short-term depression ($P < 0.05$). In contrast, no clear changes in either latency (1.90 ± 0.31 ms for EPSC1 vs. 1.98 ± 0.34 ms for EPSC2; Fig. 8*B*, *right*) or amplitude (−0.46 ± 0.13 nA for EPSC1 vs. −0.46 ± 0.14 nA for EPSC2; Fig. 8*C*, *right*) were observed for the type 2 responses ($n = 7$).

DISCUSSION

Using minimal stimulation of putative TC and CT synaptic inputs and cluster analysis and voltage-clamp characterization of evoked synaptic currents, we have demonstrated that two types of excitatory responses could be discriminated in the nRt. Type 1 responses have large amplitude, fast kinetics and propagation speed, and display short-term depression and supernormality. Type 2 responses are smaller and slower with a higher relative contribution of the NMDA component with little sensitivity to voltage-dependent Mg^{2+} block. Specific glutamate activation of thalamoreticular and corticoreticular inputs provided evidence for a TC and CT origin of the type 1 and type 2 responses, respectively.

The two types of EPSCs are likely related to inputs arising from the thalamus and cortex. The type 1 responses in our recordings have features previously suggested for TC inputs, including a large amplitude (Gentet and Ulrich 2003; Liu et al. 2001), fast axonal conduction (Beierlein and Connors 2002; Liu et al. 2001), paired pulse depression (Beierlein and Connors 2002; Gentet and Ulrich 2003), and a significant NMDA contribution, even at membrane potentials near rest (Gentet and Ulrich 2003). The type 2 EPSCs have properties consistent with those previously described for CT inputs in other systems

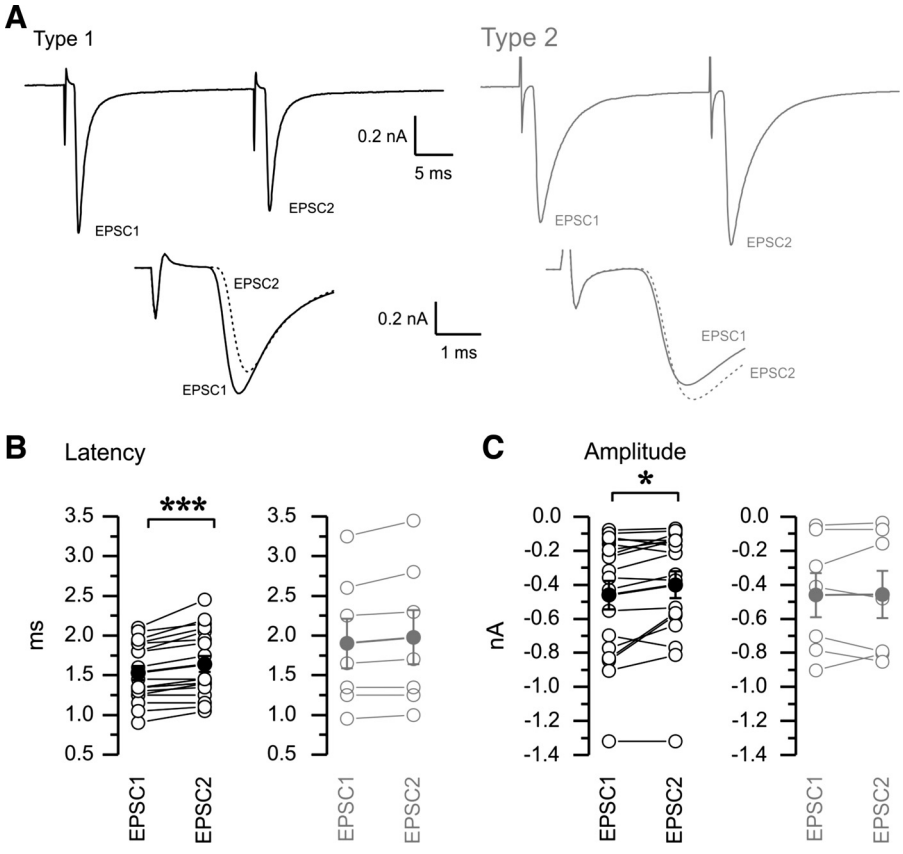

Fig. 8. Short-term plasticity properties of type 1 (black) and type 2 (gray) responses. *A*: a pair of minimal stimuli were delivered at a frequency of 40 Hz. Type 1 responses tended to show paired pulse suppression and slowing of response latency in the second pulse (*bottom* overlay of EPSC1 and EPSC2 aligned to the stimulus time), whereas type 2 responses showed little paired pulse amplitude or latency differences. *B*: population statistics for short-term latency plasticity. Paired statistical comparison showed increases in latency for the second pulse compared with the first pulse in type 1 (*left*) but not type 2 (*right*) responses. *C*: population statistics for short-term amplitude plasticity. Solid symbols with error bars represent means ± SE of individual values (*B* and *C*). The paired statistical comparison documents the paired pulse depression, i.e., decreases in amplitude for the second pulse compared with the first pulse in type 1 but not type 2 responses. Type 1: $n = 18$; type 2: $n = 7$. *$P < 0.05$; ***$P < 0.001$.

in that they were smaller than TC inputs (Gentet and Ulrich 2004) and did not show short-term depression. In addition, we showed that type 2, presumed CT, responses had a larger relative NMDAR-to-AMPAR ratio and NMDARs that were less sensitive to blockade by Mg^{2+}. CT responses showed slower EPSC kinetics, both in terms of the rise time and decay rate, as previously described (Liu et al. 2001), but also of the relatively high contribution of NMDARs at rest. Here, we provide a discriminant function that allows for the clean separation of the two types of synaptic responses based purely on the kinetics of the minimally evoked response obtained at a holding potential of −70 mV. Discriminant scores above 1 and below 0 provide unambiguous identification of synapse type, whereas values in a relatively small intermediate range of 0–1 do not. However, in this data set, only a minority of synapses (14 of 93 synapses, ~15%) produced discriminant scores. In previous studies, the properties of excitatory inputs onto the nRt were characterized mostly with current-clamp recordings, but the exact knowledge of kinetics and voltage-dependent conductance, such as AMPA and NMDA contribution, requires a reliable control of the voltage. Here, we provide the first detailed voltage-clamp analysis of TC and CT connections onto the nRt. This information will highly contribute to improve biologically realistic neural network models of TC circuits.

During direct glutamate activation of thalamic or cortical cells, the properties of the recorded sEPSCs change from baseline toward those expected by minimal electrical type 1 and type 2 responses, respectively. The small changes in population statistics after glutamate application presumably reflect the addition of new action potential-dependent EPSCs to a larger existing population of spontaneously occuring, action potential-independent EPSCs. A similar approach has been applied in immature mice in which differential sensitivity to serotonin (5-HT) of TC (sensitive) and CT (insensitive) synapses, present only during an early stage of development, was used to discriminate presumed TC and CT minimal electrical responses in the nRt into two groups (Evrard and Ropert 2009). Unfortunately, 5-HT sensitivity cannot be used in older animals, so our work confirms and extends the findings of Evrard et al. by fully characterizing the kinetics, Mg^{2+} sensitivity, and relative contributions of NMDA and AMPA receptors to CT and TC synapses in the nRt.

It has been shown that TC fibers in the cortex display subnormality (Beierlein and Connors 2002), and short-term depression has also been previously reported for cortical TC connections (Beierlein and Connors 2002) as well as for VB to nRt synapses (Gentet and Ulrich 2003), reinforcing in part the likely TC origin of our type 1 response. In contrast, supernormality and short-term facilitation have been suggested for CT axons (Beierlein and Connors 2002), but our results do not confirm this, maybe due to the small size of the type 2 sample in our study or perhaps to nonuniform properties of CT axons near to the site of origin within the cortex versus distally, far from the site of origin, in the thalamus.

Morphological basis for the distinct kinetics of type 1 and type 2 EPSCs. The slow kinetics of type 2 AMPA responses could originate in part from the electrotonic filtering that would result from a greater distance of CT than TC synapses, with the former tending to terminate on small (presumably distal) dendritic profiles (; Jones 2002; Liu and Jones 1999; Liu et al. 2001) and the latter often found to terminate on larger dendritic profiles (Liu et al. 2001). Small terminals in the nRt, presumed CT inputs, are the largest number of nRt synapses, comprising ~65% of those on distal dendrites and 50% on proximal dendrites, whereas large terminals synapses, likely derived from TC axon collaterals, were more focused on proximal dendrites, where they represent 30–40% compared with 20% on distal dendrites (Liu and Jones 1999). This distal location and spread of locations across distal and proximal locations would slow CT synaptic responses and account at least in part for the slow rise and decay times. Selective optogenetic activation of CT inputs produces responses with similar slow kinetics, reinforcing the view that type II synapses arise from CT inputs (Paz et al. 2011).

The distal location of CT synapses on nRt dendrites makes them well suited for triggering burst discharge, given the localization of T-type Ca^{2+} channels and computational studies indicating that dendritic expression is essential for the expression of long-lasting nRt bursts (Crandall et al. 2010; Destexhe et al. 1996), and AMPA and NMDARs working together may be particularly effective for this. NMDARs have recently been shown to be active at rest in nRt cells (Zhang et al. 2009), in agreement with the relatively left-shifted NMDAR *g-V* curves reported here (Fig. 5*C*), such that there is significant activation even at a membrane potential of −70 mV. In addition, the pharmacologically isolated AMPA component of the type 2 responses is also slower compared with the type 1, suggesting that the slow kinetics of type 2 EPSC at −70 mV, near rest, comes from both slow AMPA and NMDA components.

Molecular basis for the distinct properties of type 1 and type 2 EPSCs. The distinct properties between type 1 and Type 2 responses could also result from a differential expression of glutamatergic receptor subunits (Hollmann and Heinemann 1994) at TC and CT synapses and the subsequent activation of different subtypes of receptors with specific affinity, conductance, voltage dependence, or kinetics (Arrigoni and Greene 2004; Kumar and Huguenard 2003). The number of receptors expressed and activated may also be critical. For instance, the GluA4 subunit of the AMPAR (Traynelis et al. 2010) is highly expressed at CT synapses in the nRt (Golshani et al. 2001; Liu et al. 2001; Mineff and Weinberg 2000) but less in the thalamus, and this difference is responsible for a larger quantal amplitude of the EPSC in the nRt compared with the dorsal thalamus (Golshani et al. 2001). Recently, TC synapses to the nRt were found to be unaffected by inactivation of GluA4 (Paz et al. 2011), whereas CT synapses were weakened, suggesting that TC synapses are completely dependent on other AMPARs, including GluR1–GluR3. Regarding NMDARs, all NR2A–NR2D subunits are expressed in the thalamus at the postnatal stage studied here (Karavanova et al. 2007; Wenzel et al. 1996; Wenzel et al. 1997), but their distribution remains unknown at the synaptic level in the nRt. The identity of NR2 subunits confers specific affinity for glutamate and functional properties to NMDARs (Monyer et al. 1994; Vicini et al. 1998). In particular, the NR2C and NR2D subunits have been related to small sensitivity to voltage-dependent Mg^{2+} block near resting potential (Kuner and Schoepfer 1996) and could explain those of our presumed CT, type 2 responses. Moreover, it has been suggested that NR2C is likely the main contributor to NMDAR function in the nRt (Zhang et al. 2009). The slow kinetics and

small size of type 2 EPSCs could also be associated with specific subunits. Finally, the relative proportion and/or type of AMPA and NMDARs expressed at TC and CT could provide differences in the NMDA-to-AMPA ratio.

Functional strength of the putative CT and TC synaptic drive on the nRt. Type 2 responses show a strong relative contribution by NMDARs across a range of voltages, even as low as −70 mV, indicating that the voltage-dependent blockade by Mg^{2+} is incomplete and that NMDARs can be activated by synaptically released glutamate, even in the absence of depolarization produced by AMPAR activation. The voltage-clamp characterization of this strong NMDA contribution is critical for the understanding regarding cortical activation, perhaps especially in relation to absence seizure generation (Bal et al. 2000; Blumenfeld and McCormick 2000), which would then be able to provide powerful activation of the nRt to drive intense firing (Slaght et al. 2002). The latter would provide powerful inhibition of relay cells (Contreras and Steriade 1995) that could mask cortical excitatory inputs onto the thalamus (Kao and Coulter 1997) and nRt (Zhang and Jones 2004) and lead to relay cell postinhibitory rebound firing as well as recurrent excitation of nRt cells by TC inputs. This slow (NMDAR-mediated) putative CT synaptic drive on the nRt would strongly initiate activity in the intrathalamic loop. TC inputs, being powerful, may require little convergent input to the nRt to trigger firing, whereas CT inputs presumably need either temporal integration or convergence. Note that TC inputs also have a major NMDAR component but that it is relatively smaller in relation to the AMPAR component compared with CT inputs. Current-clamp recordings of unitary TC-nRt connections revealed large contributions of NMDARs to EPSPs (Gentet and Ulrich 2003), due in part to a significant AMPAR-dependent depolarization that would reduce Mg^{2+} block.

Given their large size in relation to sEPSCs, it appears that the single TC axon convergence factor could be as high as ~20 (mean amplitude ratio evoked TC EPSC to sEPSC: on average, 473 pA/24 pA) and even higher (~30) if we account for release failures. Complicating this calculation is the fact that TC terminals on nRt cells are complex, with multiple release sites (Liu et al. 2001). Together, this would suggest that approximately four to seven complex large terminal synapses, each with one to seven active zones, mediate the typical connection between each TC and nRt neuron. Cortical connections are likely mediated by a larger number of simple synapses each with a single release site and thus more distributed across the dendritic target zone of an nRt cell. The powerful feedforward inhibition observed with afferent fiber stimulation in vitro (Huguenard and Prince 1994a; Huguenard and Prince 1994b; Kao and Coulter 1997; Lam and Sherman 2010; von Krosigk et al. 1993; Warren et al. 1994) suggests that excitatory convergence, either single fiber from TC or multiple fiber from CT, is very effective in activating the nRt. TC connections are effective even at the single fiber level due to their large unitary amplitudes. CT connections can recruit nRt cell firing at least in part through their relatively greater NMDA receptor contribution that would contribute to long-lasting depolarization and the activation of multiple action potentials. Thus, either the cortex or thalamus could potentially produce the intial burst of input to nRt cells that might trigger the strong nRt firing thought to be critical in the generation of the TC circuit activity of absence epilepsy (Huguenard and McCormick 2007).

ACKNOWLEDGMENTS

The authors thank Mark Beenhakker for critical comments on the manuscript and Brian Halabisky for the assistance with cluster analysis.

Present address of C. Deleuze: INSERM U 1127, CNRS UMR 7225, Sorbonne Universités, UPMC Univ Paris 06 UMR S 1127, Institut du Cerveau et de la Moelle épinière, ICM, Paris F-75013, France.

GRANTS

This work was supported by National Institute of Neurological Disorders and Stroke Grant NS-034774.

DISCLOSURES

No conflicts of interest, financial or otherwise, are declared by the author(s).

AUTHOR CONTRIBUTIONS

C.D. and J.R.H. conception and design of research; C.D. performed experiments; C.D. and J.R.H. analyzed data; C.D. and J.R.H. interpreted results of experiments; C.D. prepared figures; C.D. and J.R.H. drafted manuscript; C.D. and J.R.H. edited and revised manuscript; C.D. and J.R.H. approved final version of manuscript.

REFERENCES

Agmon A, Connors BW. Thalamocortical responses of mouse somatosensory (barrel) cortex in vitro. *Neuroscience* 41: 365–379, 1991.

Agmon A, Connors BW. Correlation between intrinsic firing patterns and thalamocortical synaptic responses of neurons in mouse barrel cortex. *J Neurosci* 12: 319–329, 1992.

Arrigoni E, Greene RW. Schaffer collateral and perforant path inputs activate different subtypes of NMDA receptors on the same CA1 pyramidal cell. *Br J Pharmacol* 142: 317–322, 2004.

Avanzini G, Vergnes M, Spreafico R, Marescaux C. Calcium-dependent regulation of genetically determined spike and waves by the reticular thalamic nucleus of rats. *Epilepsia* 34: 1–7, 1993.

Bal T, Debay D, Destexhe A. Cortical feedback controls the frequency and synchrony of oscillations in the visual thalamus. *J Neurosci* 20: 7478–7488, 2000.

Beierlein M, Connors BW. Short-term dynamics of thalamocortical and intracortical synapses onto layer 6 neurons in neocortex. *J Neurophysiol* 88: 1924–1932, 2002.

Blumenfeld H, McCormick DA. Corticothalamic inputs control the pattern of activity generated in thalamocortical networks. *J Neurosci* 20: 5153–5162, 2000.

Bourassa J, Pinault D, Deschênes M. Corticothalamic projections from the cortical barrel field to the somatosensory thalamus in rats: a single-fibre study using biocytin as an anterograde tracer. *Eur J Neurosci* 7: 19–30, 1995.

Chen L, Huang LY. Protein kinase C reduces Mg^{2+} block of NMDA-receptor channels as a mechanism of modulation. *Nature* 356: 521–523, 1992.

Contreras D, Steriade M. Cellular basis of EEG slow rhythms: a study of dynamic corticothalamic relationships. *J Neurosci* 15: 604–622, 1995.

Cox CL, Huguenard JR, Prince DA. Nucleus reticularis neurons mediate diverse inhibitory effects in thalamus. *Proc Natl Acad Sci USA* 94: 8854–8859, 1997.

Crabtree JW. Organization in the somatosensory sector of the cat's thalamic reticular nucleus. *J Comp Neurol* 366: 207–222, 1996.

Crabtree JW, Collingridge GL, Isaac JT. A new intrathalamic pathway linking modality-related nuclei in the dorsal thalamus. *Nat Neurosci* 1: 389–394, 1998.

Crandall SR, Govindaiah G, Cox CL. Low-threshold Ca^{2+} current amplifies distal dendritic signaling in thalamic reticular neurons. *J Neurosci* 30: 15419–15429, 2010.

Cruikshank SJ, Urabe H, Nurmikko AV, Connors BW. Pathway-specific feedforward circuits between thalamus and neocortex revealed by selective optical stimulation of axons. *Neuron* 65: 230–245, 2010.

Deleuze C, Huguenard JR. Distinct electrical and chemical connectivity maps in the thalamic reticular nucleus: potential roles in synchronization and sensation. *J Neurosci* 26: 8633–8645, 2006.

Destexhe A, Contreras D, Steriade M, Sejnowski TJ, Huguenard JR. In vivo, in vitro and computational analysis of dendritic calcium currents in thalamic reticular neurons. *J Neurosci* 16: 169–185, 1996.

Evrard A, Ropert N. Early development of the thalamic inhibitory feedback loop in the primary somatosensory system of the newborn mice. *J Neurosci* 29: 9930–9940, 2009.

Friedberg EB, Ross DT. Degeneration of rat thalamic reticular neurons following intrathalamic domoic acid injection. *Neurosci Lett* 151: 115–119, 1993.

Gentet LJ, Ulrich D. Strong, reliable and precise synaptic connections between thalamic relay cells and neurones of the nucleus reticularis in juvenile rats. *J Physiol* 546: 801–811, 2003.

Gentet LJ, Ulrich D. Electrophysiological characterization of synaptic connections between layer VI cortical cells and neurons of the nucleus reticularis thalami in juvenile rats. *Eur J Neurosci* 19: 625–633, 2004.

Golshani P, Liu XB, Jones EG. Differences in quantal amplitude reflect GluR4-subunit number at corticothalamic synapses on two populations of thalamic neurons. *Proc Natl Acad Sci U S A* 98: 4172–4177, 2001.

Halabisky B, Shen F, Huguenard JR, Prince DA. Electrophysiological classification of somatostatin-positive interneurons in mouse sensorimotor cortex. *J Neurophysiol* 96: 834–845, 2006.

Harris RM. Axon collaterals in the thalamic reticular nucleus from thalamocortical neurons of the rat ventrobasal thalamus. *J Comp Neurol* 258: 397–406, 1987.

Hartings JA, Temereanca S, Simons DJ. High responsiveness and direction sensitivity of neurons in the rat thalamic reticular nucleus to vibrissa deflections. *J Neurophysiol* 83: 2791–2801, 2000.

Hartings JA, Temereanca S, Simons DJ. State-dependent processing of sensory stimuli by thalamic reticular neurons. *J Neurosci* 23: 5264–5271, 2003.

Hollmann M, Heinemann S. Cloned glutamate receptors. *Annu Rev Neurosci* 17: 31–108, 1994.

Huguenard JR, McCormick DA. Thalamic synchrony and dynamic regulation of global forebrain oscillations. *Trends Neurosci* 30: 350–356, 2007.

Huguenard JR, Prince DA. A novel T-type current underlies prolonged Ca^{2+}-dependent burst firing in GABAergic neurons of rat thalamic reticular nucleus. *J Neurosci* 12: 3804–3817, 1992.

Huguenard JR, Prince DA. Clonazepam suppresses $GABA_B$-mediated inhibition in thalamic relay neurons through effects in nucleus reticularis. *J Neurophysiol* 71: 2576–2581, 1994a.

Huguenard JR, Prince DA. Intrathalamic rhythmicity studied in vitro: nominal T current modulation causes robust anti-oscillatory effects. *J Neurosci* 14: 5485–5502, 1994b.

Jacobsen RB, Ulrich D, Huguenard JR. $GABA_B$ and NMDA receptors contribute to spindle-like oscillations in rat thalamus in vitro. *J Neurophysiol* 86: 1365–1375, 2001.

Jacobson S. Sequence of myelinization in the brain of the albino rat. A. Cerebral cortex, thalamus and related structures. *J Comp Neurol* 121: 5–29, 1963.

Jones EG. Thalamic circuitry and thalamocortical synchrony. *Philos Trans R Soc Lond B Biol Sci* 357: 1659–1673, 2002.

Jones EG, Powell TP. The cortical projection of the ventroposterior nucleus of the thalamus in the cat. *Brain Res* 13: 298–318, 1969.

Kao CQ, Coulter DA. Physiology and pharmacology of corticothalamic stimulation-evoked responses in rat somatosensory thalamic neurons in vitro. *J Neurophysiol* 77: 2661–2676, 1997.

Karavanova I, Vasudevan K, Cheng J, Buonanno A. Novel regional and developmental NMDA receptor expression patterns uncovered in NR2C subunit-β-galactosidase knock-in mice. *Mol Cell Neurosci* 34: 468–480, 2007.

Kolhekar R, Murphy S, Gebhart GF. Thalamic NMDA receptors modulate inflammation-produced hyperalgesia in the rat. *Pain* 71: 31–40, 1997.

Kumar SS, Huguenard JR. Pathway-specific differences in subunit composition of synaptic NMDA receptors on pyramidal neurons in neocortex. *J Neurosci* 23: 10074–10083, 2003.

Kuner T, Schoepfer R. Multiple structural elements determine subunit specificity of Mg^{2+} block in NMDA receptor channels. *J Neurosci* 16: 3549–3558, 1996.

Lam YW, Sherman SM. Functional organization of the somatosensory cortical layer 6 feedback to the thalamus. *Cereb Cortex* 20: 13–24, 2010.

Landisman CE, Long MA, Beierlein M, Deans MR, Paul DL, Connors BW. Electrical synapses in the thalamic reticular nucleus. *J Neurosci* 22: 1002–1009, 2002.

Leresche N, Lambert RC, Errington AC, Crunelli V. From sleep spindles of natural sleep to spike and wave discharges of typical absence seizures: is the hypothesis still valid? *Pflugers Arch* 463: 201–212, 2012.

Liu XB, Jones EG. Predominance of corticothalamic synaptic inputs to thalamic reticular nucleus neurons in the rat. *J Comp Neurol* 414: 67–79, 1999.

Liu XB, Bolea S, Golshani P, Jones EG. Differentiation of corticothalamic and collateral thalamocortical synapses on mouse reticular nucleus neurons by EPSC amplitude and AMPA receptor subunit composition. *Thalamus Related Syst* 1: 15–29, 2001.

Marie H, Morishita W, Yu X, Calakos N, Malenka RC. Generation of silent synapses by acute in vivo expression of CaMKIV and CREB. *Neuron* 45: 741–752, 2005.

Mayer ML, Vyklicky L Jr, Westbrook GL. Modulation of excitatory amino acid receptors by group IIB metal cations in cultured mouse hippocampal neurones. *J Physiol* 415: 329–350, 1989.

Meeren HK, Pijn JP, Van Luijtelaar EL, Coenen AM, Lopes da Silva FH. Cortical focus drives widespread corticothalamic networks during spontaneous absence seizures in rats. *J Neurosci* 22: 1480–1495, 2002.

Meeren HK, Veening JG, Moderscheim TA, Coenen AM, Van Luijtelaar G. Thalamic lesions in a genetic rat model of absence epilepsy: dissociation between spike-wave discharges and sleep spindles. *Exp Neurol* 217: 25–37, 2009.

Mineff EM, Weinberg RJ. Differential synaptic distribution of AMPA receptor subunits in the ventral posterior and reticular thalamic nuclei of the rat. *Neuroscience* 101: 969–982, 2000.

Monyer H, Burnashev N, Laurie DJ, Sakmann B, Seeburg PH. Developmental and regional expression in the rat brain and functional properties of four NMDA receptors. *Neuron* 12: 529–540, 1994.

Myme CI, Sugino K, Turrigiano GG, Nelson SB. The NMDA-to-AMPA ratio at synapses onto layer 2/3 pyramidal neurons is conserved across prefrontal and visual cortices. *J Neurophysiol* 90: 771–779, 2003.

Nowak L, Bregestovski P, Ascher P, Herbet A, Prochiantz A. Magnesium gates glutamate-activated channels in mouse central neurones. *Nature* 307: 462–465, 1984.

Ohara PT, Lieberman AR. The thalamic reticular nucleus of the adult rat: experimental anatomical studies. *J Neurocytol* 14: 365–411, 1985.

Olsen SR, Bortone DS, Adesnik H, Scanziani M. Gain control by layer six in cortical circuits of vision. *Nature* 483: 47–52, 2012.

Paz JT, Bryant AS, Peng K, Fenno L, Yizhar O, Frankel WN, Deisseroth K, Huguenard JR. A new mode of corticothalamic transmission revealed in the $Gria4^{-/-}$ model of absence epilepsy. *Nat Neurosci* 14: 1167–1173, 2011.

Pinault D. The thalamic reticular nucleus: structure, function and concept. *Brain Res Brain Res Rev* 46: 1–31, 2004.

Ranck JB Jr. Which elements are excited in electrical stimulation of mammalian central nervous system: a review. *Brain Res* 98: 417–440, 1975.

Ross DT, Brasko J, Patrikios P. The AMPA antagonist NBQX protects thalamic reticular neurons from degeneration following cardiac arrest in rats. *Brain Res* 683: 117–128, 1995.

Salami M, Itami C, Tsumoto T, Kimura F. Change of conduction velocity by regional myelination yields constant latency irrespective of distance between thalamus and cortex. *Proc Natl Acad Sci USA* 100: 6174–6179, 2003.

Scheibel ME, Scheibel AB. The organization of the nucleus reticularis thalami: a Golgi study. *Brain Res* 1: 43–62, 1966.

Shu Y, McCormick DA. Inhibitory interactions between ferret thalamic reticular neurons. *J Neurophysiol* 87: 2571–2576, 2002.

Slaght SJ, Leresche N, Deniau JM, Crunelli V, Charpier S. Activity of thalamic reticular neurons during spontaneous genetically determined spike and wave discharges. *J Neurosci* 22: 2323–2334, 2002.

Steriade M, McCormick DA, Sejnowski TJ. Thalamocortical oscillations in the sleeping and aroused brain. *Science* 262: 679–685, 1993.

Swadlow HA. Systematic variations in the conduction velocity of slowly conducting axons in the rabbit corpus callosum. *Exp Neurol* 43: 445–451, 1974.

Swadlow HA. Efferent neurons and suspected interneurons in S-1 forelimb representation of the awake rabbit: receptive fields and axonal properties. *J Neurophysiol* 63: 1477–1498, 1990.

Swett JE, Bourassa CM. Electrical stimulation of peripheral nerve. In: *Electrical Stimulation Research Techniques*, edited by Patterson MM, Kesner RP. New York: Academic, 1981, p. 274–281.

Thorndike RL. Who belongs in the family? *Pshcometrika* 18: 267–276, 1953.

Traynelis SF, Wollmuth LP, McBain CJ, Menniti FS, Vance KM, Ogden KK, Hansen KB, Yuan H, Myers SJ, Dingledine R. Glutamate receptor ion channels: structure, regulation, and function. *Pharmacol Rev* 62: 405–496, 2010.

Tsumoto T, Suda K. Laminar differences in development of afferent innervation to striate cortex neurones in kittens. *Exp Brain Res* 45: 433–446, 1982a.

Tsumoto T, Suda K. Postnatal development of the corticofugal projection from striate cortex to lateral geniculate nucleus in kittens. *Brain Res* 256: 323–332, 1982b.

Vicini S, Wang JF, Li JH, Zhu WJ, Wang YH, Luo JH, Wolfe BB, Grayson DR. Functional and pharmacological differences between recombinant *N*-methyl-D-aspartate receptors. *J Neurophysiol* 79: 555–566, 1998.

von Krosigk M, Bal T, McCormick DA. Cellular mechanisms of a synchronized oscillation in the thalamus. *Science* 261: 361–364, 1993.

Warren RA, Agmon A, Jones EG. Oscillatory synaptic interactions between ventroposterior and reticular neurons in mouse thalamus in vitro. *J Neurophysiol* 72: 1993–2003, 1994.

Warren RA, Jones EG. Maturation of neuronal form and function in a mouse thalamo-cortical circuit. *J Neurosci* 17: 277–295, 1997.

Wenzel A, Fritschy JM, Mohler H, Benke D. NMDA receptor heterogeneity during postnatal development of the rat brain: differential expression of the NR2A, NR2B, and NR2C subunit proteins. *J Neurochem* 68: 469–478, 1997.

Wenzel A, Villa M, Mohler H, Benke D. Developmental and regional expression of NMDA receptor subtypes containing the NR2D subunit in rat brain. *J Neurochem* 66: 1240–1248, 1996.

Yizhar O, Fenno LE, Prigge M, Schneider F, Davidson TJ, O'Shea DJ, Sohal VS, Goshen I, Finkelstein J, Paz JT, Stehfest K, Fudim R, Ramakrishnan C, Huguenard JR, Hegemann P, Deisseroth K. Neocortical excitation/inhibition balance in information processing and social dysfunction. *Nature* 477: 171–178, 2011.

Zhang L, Jones EG. Corticothalamic inhibition in the thalamic reticular nucleus. *J Neurophysiol* 91: 759–766, 2004.

Zhang Y, Llinas RR, Lisman JE. Inhibition of NMDARs in the nucleus reticularis of the thalamus produces delta frequency bursting. *Front Neural Circuits* 3: 20, 2009.